

1 **The effects of nitrate on the heterogeneous uptake of sulfur dioxide on**  
2 **hematite**

3 L. D. Kong, X. Zhao, Z. Y. Sun, Y. W. Yang, H. B. Fu, X. Yang, S. C. Zhang, J. M.  
4 Chen, L. Wang, and T. T. Cheng

5 Shanghai Key Laboratory of Atmospheric Particle Pollution and Prevention, Department  
6 of Environmental Science & Engineering, Fudan University, Shanghai 200433, China

7 Lingdong Kong: [ldkong@fudan.edu.cn](mailto:ldkong@fudan.edu.cn) (corresponding author)

8

9

10

11

12

13

14

15

16

17

18

19

20

21 **Abstract.** Nitrate is often found to be associated with atmospheric particles. Surface  
22 nitrate can change the hygroscopicity of these particles, and thus impact their chemical  
23 reactivity. However, the influence of nitrate on heterogeneous reactions of atmospheric  
24 trace gases is poorly understood. In this work, the effects of nitrate on heterogeneous  
25 conversion of SO<sub>2</sub> with hematite at 298 K are investigated using an in situ diffuse  
26 reflectance infrared Fourier transform spectroscopy (DRIFTS) and a White cell coupled  
27 with Fourier transform infrared spectroscopy (White cell-FTIR). It is found that nitrate  
28 participates in heterogeneous reactions of SO<sub>2</sub>, accelerates the formation rate of sulfate,  
29 and leads to the formation of surface-adsorbed HNO<sub>3</sub> and gas-phase N<sub>2</sub>O and HONO.  
30 The results indicate that low to moderate amounts of nitrate significantly enhance the  
31 reactivity of hematite-nitrate mixtures, the uptake of SO<sub>2</sub> and the formation of sulfate on  
32 hematite. For mixtures, the sample containing 24% nitrate exhibits the highest sulfate  
33 formation rate, and its corresponding uptake coefficient calculated by geometric surface  
34 area is about 5.5 times higher than that of hematite alone. The sample containing 48%  
35 nitrate presents the highest BET uptake coefficient, and the value is about 8 times higher  
36 than that of pure hematite. No uptake of SO<sub>2</sub> and formation of sulfate are observed on  
37 pure nitrate. Evidence presented herein implies a significant contribution of the  
38 unreleased HNO<sub>3</sub> and HONO in the particles for the conversion of SO<sub>2</sub> and the enhanced  
39 formation of sulfate in the atmosphere. A possible mechanism for the influence of nitrate  
40 on the heterogeneous conversion of SO<sub>2</sub> on hematite is proposed, and atmospheric  
41 implications based on these results are discussed.

42

43

## 44 **1 Introduction**

45 Sulfur dioxide is a major component of air pollution. It is usually generated by the  
46 combustion of fossil fuels and by the atmospheric oxidation of biogenic organic sulfur  
47 compounds, particularly dimethyl sulfide. The oxidation of sulfur dioxide leads to sulfate  
48 particulate formation. Atmospheric sulfate particles play significant roles in adverse  
49 health effects, visibility degradation and rain water acidification (Seinfeld and Pandis,  
50 2006). The conversion of SO<sub>2</sub> to sulfate in the atmosphere usually occurs via three well-  
51 known pathways, including gas-phase oxidation to sulfuric acid followed by  
52 condensation into the particulate-phase, aqueous-phase oxidation in cloud and fog  
53 droplets, and various heterogeneous reactions on the surfaces of aerosol particles  
54 (Kerminen et al., 2000). There have been a number of atmospheric chemistry models  
55 applied to predict the formation of sulfate aerosols on a global scale (Kasibhatla et al.,  
56 1997; Laskin et al., 2003). The results suggest that atmospheric SO<sub>2</sub> concentrations are  
57 typically overestimated while sulfate concentrations tend to be underestimated  
58 (Kasibhatla et al., 1997; Laskin et al., 2003), and the two pathways including gaseous  
59 oxidation by OH radical and aqueous oxidation in cloud and fog droplets by ozone and  
60 hydrogen peroxide are insufficient to bridge the gap between field and modeling studies  
61 (Luria and Sievering, 1991). Including in-cloud oxidation catalyzed by natural transition  
62 metal ions in models will improve agreement between models and observations (Harris et  
63 al., 2013). These imply that the heterogeneous conversion of SO<sub>2</sub> to sulfate on aerosols  
64 may make an important contribution to the atmospheric sulfate concentration, or there are  
65 some unknown pathways for the formation of sulfate in the troposphere. The  
66 heterogeneous oxidation of SO<sub>2</sub> to sulfate on aerosols has therefore received increasing

67 attention in recent years. To date there have been a lot of studies regarding heterogeneous  
68 reactions of SO<sub>2</sub> on various model oxides and mineral dust particles (Dentener et al.,  
69 1996; Goodman et al., 2001; Usher et al., 2002; Ullerstam et al., 2003; Baltrusaitis et al.,  
70 2007; Lin et al., 2010; Zhu et al., 2011; Wu et al., 2011; Liu et al., 2012). However, the  
71 atmospheric heterogeneous reactions of SO<sub>2</sub> still have large uncertainties (Laskin et al.,  
72 2003), and the underlying mechanisms of sulfate formation on mineral aerosols are not  
73 completely understood (Dentener et al., 1996). For example, in the atmosphere, the  
74 heterogeneous reactions of SO<sub>2</sub> are unavoidably affected by other atmospheric species,  
75 but little attention has been paid to the effects of other species on the heterogeneous  
76 reaction of SO<sub>2</sub> in the laboratory studies up to now (Ullerstam et al., 2003; Lin et al.,  
77 2010; Wu et al., 2011; Liu et al., 2012).

78 Mineral dust aerosol, emitted from the arid and semiarid regions with a global source  
79 strength of about 1000-3000 Tg yr<sup>-1</sup>, is one of the most important contributors to the  
80 airborne particulate matter (Dentener et al., 1996). It is now widely recognized that  
81 mineral dust aerosols provide reactive surfaces for atmospheric trace gases, and the  
82 reactions on mineral dust particles change their sizes, optical and hygroscopic properties  
83 as well as lifetime in the atmosphere, which, in turn, can change the climate impact of  
84 these particles. Mineral oxide represents an important and reactive component of mineral  
85 dust aerosol. Being one of the typical oxide minerals, Fe<sub>2</sub>O<sub>3</sub> contributes ~6% by mass to  
86 the total dust burden in the atmosphere (Usher et al., 2003). Atmospheric chemical  
87 processing of Fe-containing dust particles during long-range transport can impact the  
88 amount of soluble iron (Zhuang et al., 1992; Meskhidze et al., 2003), while soluble iron  
89 will limit phytoplankton primary productivity in extensive regions of the ocean referred

90 to as high-nutrient low-chlorophyll regions (Moore et al., 2002), which ultimately has  
91 implications for global climate as well as carbon and nitrogen cycles (Jickells and Spokes,  
92 2001). Thus, there is interest in the atmospheric chemistry of  $\text{Fe}_2\text{O}_3$ . On the other hand,  
93 field studies have also observed that nitrate is one of the most common components of  
94 secondary particles. It's often found to be associated with these mineral dust particles in  
95 the atmosphere (Dentener et al., 1996). Surface nitrate enhances hygroscopic properties  
96 of original particles and, in turn, changes their physicochemical properties (Hoffman et  
97 al., 2004). This will inevitably impact their chemical reactivity, and therefore lead to a  
98 remarkable difference in their heterogeneous chemistry. However, little attention has  
99 been paid to the influence of nitrate on heterogeneous reactions of  $\text{SO}_2$  on atmospheric  
100 aerosols up to now (Lin et al., 2010).

101 In the present study, the effects of nitrate on heterogeneous conversions of  $\text{SO}_2$  on  
102 mineral particles at room temperature are investigated using an in situ diffuse reflectance  
103 infrared Fourier transform spectroscopy (DRIFTS) and a White cell coupled with Fourier  
104 transform infrared spectroscopy (White cell-FTIR). Hematite ( $\alpha\text{-Fe}_2\text{O}_3$ , one of the typical  
105 components in mineral aerosol) and sodium nitrate (a major form of nitrate in sea-salt  
106 particles) were used as model components of particles. The heterogeneous conversion  
107 mechanism of  $\text{SO}_2$  is proposed and atmospheric implications of the present study are  
108 discussed. The results reveal a potential pathway of sulfate formation in the troposphere  
109 and the significant contribution of particulate nitrate for the conversion of  $\text{SO}_2$  and the  
110 enhanced formation of sulfate in the atmosphere.

## 111 **2 Experimental**

## 112 **2.1 Materials**

113 Hematite was prepared according to the procedure reported previously (Schwertmann and  
114 Cornell, 2000). Powder X-ray diffraction confirmed the prepared sample as pure hematite  
115 (Fig. S1 in the Supplement). The Brunauer-Emmett-Teller (BET) surface area was 12.1  
116  $\text{m}^2 \text{g}^{-1}$  (Micromeritics TriStar 3000, Micromeritics Instrument Co., USA.). Sodium nitrate  
117 (Analytical grade, Shanghai Ab Chem Co. Ltd.) was used without further purification.  
118 Gaseous oxygen, argon (99.999% purity, Shanghai Yunguang Specialty Gases Inc.), and  
119  $\text{SO}_2$  (97 ppm,  $\text{SO}_2/\text{N}_2$ , Shanghai Yunguang Specialty Gases Inc.) were introduced  
120 through an air-dryer before use.

121 In order to systematically study the effects of nitrate on heterogeneous reactions of  
122  $\text{SO}_2$  with atmospheric aerosols, a series of hematite-sodium nitrate mixtures with the  
123 mass fractions of sodium nitrate in the mixtures in the range of 2-90% (w/w) (denoted as  
124 FN-2, FN-6, ..., FN-90, respectively) were prepared. Hematite was impregnated with a  
125 saturated aqueous solution of sodium nitrate, and then the mixtures were stirred manually  
126 and dried under an infrared lamp. Considering that aerosol particles in the real  
127 atmosphere invariably contain surface-adsorbed water and the surface-adsorbed water  
128 plays an important role in the heterogeneous chemistry of atmospheric  $\text{SO}_2$ , all of the  
129 prepared samples were kept in a desiccator at 68% relative humidity (RH) for 48 h before  
130 further use. Powder X-ray diffraction indicated that no secondary processes occurred on  
131 the hematite surface during the sample preparation and the subsequent sample  
132 equilibration (see Fig. S1 in the Supplement). The humid samples including the hematite-  
133 nitrate mixtures, pure hematite and nitrate were still loose fine powders after the

134 equilibration, and this treatment made some adsorbed water molecule layers be present on  
135 the samples.

## 136 **2.2 In situ DRIFTS experiments**

137 In situ DRIFTS spectra were recorded using a Nicolet Avatar 360 FTIR spectrometer,  
138 equipped with a high-sensitivity mercury cadmium telluride (MCT) detector and a  
139 Spectra-Tech diffuse reflectance accessory, as described previously (Fu et al., 2007; also  
140 see Fig. S2 in the Supplement). The DRIFTS sample cell is coupled with a temperature  
141 controller. A 30-mg sample was placed into the ceramic sample holder in the in situ  
142 chamber, and the sample temperature controller was used to control reaction temperature.  
143 Before the reaction gas was introduced, the reaction chamber was purged with argon (100  
144 mL/min) for 1 h, and then a background spectrum of the unreacted powder sample was  
145 collected. Subsequently, a mixture of SO<sub>2</sub> (e.g. 3 ppm) and O<sub>2</sub> (21% v/v) with argon  
146 carrier was introduced into the chamber at a total flow rate of 100 mL/min, and then IR  
147 spectra were collected as a function of reaction time. The total reaction time is about 4-6  
148 h. All spectra reported here were recorded at a resolution of 4 cm<sup>-1</sup> for 100 scans. All of  
149 the measurements were repeated three times. In addition, it should be pointed out that  
150 weak surface water loss will be observed during the purge process, but the loss of water is  
151 almost stopped after about 40 min. Furthermore, less water loss is also observed after the  
152 introduction of the reactive gases. These imply that some water molecules are kept in the  
153 sample due to the presence of hygroscopic salt (NaNO<sub>3</sub>).

## 154 **2.3 In situ White cell-FTIR experiments**

155 An infrared cell (White cell reactor, Model 19-V, a variable-path long path cell with the  
156 optical path length from 2.4 to 24 m. Infrared Analysis, Inc.) coupled to a Fourier  
157 transform infrared spectrometer was used to measure trace gaseous reactants and the  
158 possible gaseous products formed from the heterogeneous reaction of SO<sub>2</sub>. The optical  
159 path length was set to the maximum for all of the measurements. The infrared cell was  
160 cleaned by ultra-pure water and then dried before every experiment. The infrared cell was  
161 connected to a vacuum system and a gas supply system. The apparatus has been  
162 described in detail elsewhere (Fu et al., 2007; Zhang et al., 2006; also see Fig. S3 in the  
163 Supplement). For in situ FTIR measurements, the experiments were conducted in the  
164 absence of light. The infrared cell was flushed with pure argon with the aid of the vacuum  
165 system, and this cleaning process was repeated three times before a sample was placed  
166 into the infrared cell. A 30-mg sample was placed in a small reaction disc (inner diameter  
167 = 1 cm, depth = 0.1 cm) made of quartz, and then the disc was placed into the infrared  
168 cell. After the sample was placed, argon was filled into the cell again to  $1.01 \times 10^5$  Pa, the  
169 background spectrum of the gases was collected, and then the infrared cell was evacuated  
170 to 20 Pa again. Argon was used as a carrier gas to load the reactive gases SO<sub>2</sub> and O<sub>2</sub> into  
171 the infrared cell through the gas supply system. After the infrared cell was filled to a  
172 pressure of  $1.01 \times 10^5$  Pa, it remained at that pressure for 3 min to ensure homogeneous  
173 mixing of the gases in the infrared cell before starting to collect the in situ IR spectra.  
174 FTIR spectra were recorded using a Nicolet Avatar 360 FTIR equipped with a liquid  
175 nitrogen cooled MCT detector. 100 repeat spectral scans were averaged over a range of  
176 600-4000 cm<sup>-1</sup> at a spectral resolution of 4 cm<sup>-1</sup>. A single-beam spectrum collected prior  
177 to the SO<sub>2</sub> exposure was used as the reference spectrum. In order to trace gaseous



178 products, a long reaction time (up to 20 h) was adopted in some experiments. The peak  
179 areas of the characteristic peaks of SO<sub>2</sub> have a linear correlation with the concentration of  
180 SO<sub>2</sub> ( $R^2 > 0.999$ ). Thus, the concentration of gaseous SO<sub>2</sub> can be determined by  
181 measuring the corresponding in situ FTIR spectra peak areas of gaseous SO<sub>2</sub>. All of the  
182 measurements were repeated at least twice.

#### 183 **2.4 Heterogeneous reaction of SO<sub>2</sub> in the dark**

184 Heterogeneous reactions of SO<sub>2</sub> (50 ppm) on humid hematite, FN-24 and FN-90 were  
185 performed in the presence of O<sub>2</sub> (21% v/v) in three 42 mL brown glass bottles in the dark  
186 at room temperature for about 3-7 days, respectively. An about 30 mg sample, which was  
187 kept in a desiccator at 68% RH for 48 h, was placed flatly on the bottom of the glass  
188 bottle, in order to make sure that no sample particles were stuck on the interior wall of  
189 glass bottle. Before the reaction gas SO<sub>2</sub> was introduced, a mixture of Ar and O<sub>2</sub> (21%  
190 v/v) was introduced into the bottle at a total flow rate of 100 mL/min to expel air from the  
191 bottle for an hour, after which the inlet and the outlet of the bottle were closed. Then 2.1  
192 μL of SO<sub>2</sub> (50 ppm) was injected through the septum into the bottle with a microsyringe.  
193 After the above treatments, the final amount of water in the bottle should be close to that  
194 in the same sample in the DRIFTS cell. The bottle was packed in aluminum foil and then  
195 placed in the dark for 3-7 days.

#### 196 **2.5 Ion analysis and N<sub>2</sub>O detection**

197 The products formed on the sample surface were analyzed by ion chromatography after  
198 DRIFTS experiments. The method is similar to that in a previous study (Ullerstam et al.,  
199 2002). The reacted sample particles were extracted by sonication with ultrapure water

200 (specific resistance  $\geq 18.0 \text{ M}\Omega\text{-cm}$ ). The leaching solution contained 1% formaldehyde as  
201 a preservative to suppress sulfite oxidation and was obtained through a  $0.45 \mu\text{m}$  PTFE  
202 membrane filter. The filtered solution was analyzed using a Dionex DX 500 ion  
203 chromatography, which was equipped with a Dionex AS 14 analytical column and a  
204 CD20 conductivity detector. A weak base eluent ( $1.0 \text{ mM NaHCO}_3$  -  $3.5 \text{ mM Na}_2\text{CO}_3$ )  
205 was used for anion detection at a flow rate of  $1.5 \text{ mL/min}$ . Quality assurance of species  
206 measurement was routinely carried out by using standard reference materials produced by  
207 the National Research Center for Certified Reference Materials, China.

208 A solid phase microextraction-gas chromatography-mass spectrometry (SPME-GC-MS)  
209 method was also used to detect nitrous oxide (Drescher et al., 2006). SPME was carried  
210 out using a commercial SUPELCO  $75 \mu\text{m}$  Carboxen/PDMS fiber to qualitatively analyze  
211  $\text{N}_2\text{O}$ . Before the fiber was used for the first time, the fiber was conditioned at  $280 \text{ }^\circ\text{C}$  until  
212 a clean chromatogram was obtained under normal run conditions. In addition, to  
213 minimize background signals, the fibers were heated in the GC inlet for 2 to 5 minutes  
214 before each sampling. The SPME fiber was directly inserted in the White Cell reactor or  
215 brown glass bottle for 30 min at room temperature for the collection of gas-phase  $\text{N}_2\text{O}$ .  
216 The analysis was performed using a GC-MS (Agilent, USA) fused-silica capillary  
217 column (HP-5MS, J & W Scientific, Folsom, CA, USA,  $30 \text{ m} \times 0.25 \text{ mm I.D.}$ ,  $0.25 \mu\text{m}$   
218 film thickness). The carrier gas was high purity helium (99.999%,  $1.0 \text{ mL/min}$ ). The  
219 mass spectrometer was operated in the electron ionization (EI) mode at the electron  
220 energy of  $70 \text{ eV}$ . Thermal desorption of retained compounds on fiber was carried out at  
221  $260 \text{ }^\circ\text{C}$  in splitless mode. A blank analysis was performed prior to running a sample  
222 analysis.

## 223 **3 Results and discussion**

### 224 **3.1 Effect of nitrate on surface species formed from the uptake of SO<sub>2</sub> onto hematite**

225 In situ DRIFTS experiments were carried out on humid hematite, pure nitrate and a series  
226 of hematite-sodium nitrate mixtures with 2-90% of mass fractions of nitrate, respectively.  
227 Each experiment was performed at 298 K with 30 mg of sample to investigate the effects  
228 of nitrate on the uptake of gas-phase SO<sub>2</sub> onto the sample particle surface and the nature  
229 of the formed surface-bound species.

#### 230 **3.1.1 Surface sulfur-containing species**

231 Figure 1a shows the in situ DRIFT spectra of surface species produced on pure hematite  
232 after exposure to SO<sub>2</sub>. Four prominent peaks at 1261, 1219, 1158 and 1056 cm<sup>-1</sup> and three  
233 weak shoulder peaks at 1361, 1337 and 1000 cm<sup>-1</sup> are readily observed in the spectra. The  
234 intensities of these peaks increase as the reaction proceeds. These peaks can be assigned  
235 to adsorbed bisulfate and/or sulfate on the particle surface based on assignments in  
236 previous studies (Yamaguchi et al., 1986; Watanabe et al., 1994; Persson and Lovgren,  
237 1996; Hug, 1997; Sugimoto and Wang, 1998; Nanayakkara et al., 2012). Watanabe *et al*  
238 observed infrared absorption peaks at 1360, 1270, 1150 and 1020 cm<sup>-1</sup> for the sulfated  
239 hematite at 25 °C (Watanabe et al., 1994), and suggested that the peak at 1270 cm<sup>-1</sup> was  
240 assigned to the symmetric stretching vibration mode of S=O and the peak at 1150 cm<sup>-1</sup>  
241 was assigned to the asymmetric stretching vibration mode of S-O. A transmission FTIR  
242 study on SO<sub>2</sub> reacted TiO<sub>2</sub> surface has also shown peaks at 1361, 1297, 1172, 1116, 1050  
243 and 1000 cm<sup>-1</sup>, which were assigned to adsorbed sulfate species. The peak at 1335 cm<sup>-1</sup>  
244 was also observed by Nanayakkara *et al.* and was thought to be most likely due to the

245 formation of sulfate (Nanayakkara et al., 2012). Therefore, in the present study, the  
246 prominent peaks at 1261, 1158, 1056 and 1000  $\text{cm}^{-1}$  reflect the formation of adsorbed  
247 sulfate. Additionally, peak fitting using a combination of Lorentzian and Gaussian  
248 lineshapes to deconvolute overlapping peaks of every single spectrum of an experiment  
249 shows that the peaks at 1261 and 1158  $\text{cm}^{-1}$  simultaneously increase in intensity as the  
250 reaction time increases, while the peak at 1219  $\text{cm}^{-1}$  shows a completely different  
251 behavior (see Fig. S4 in the Supplement). The peak at 1219  $\text{cm}^{-1}$  rapidly grows in the  
252 early stage of the reaction, reaches a plateau, and then slightly decreases in intensity as  
253 the reaction proceeds, implying that the peak at 1219  $\text{cm}^{-1}$  should be assigned to different  
254 surface species and this species undergoes secondary chemistry on the sample surface.  
255 Faguy *et al* studied the structure of bisulfate and sulfate adsorbed on the Pt (111) surface  
256 by potential difference Fourier transform infrared spectroscopy and found that a  
257 maximum at 1227-1250  $\text{cm}^{-1}$  was consistent with adsorbed bisulfate or adsorbed sulfate-  
258  $\text{H}_3\text{O}^+$  ternary complexes on the Pt (111) electrode surface (Faguy and Marinković, 1996).  
259 Hug (1997) found that a peak at or above 1200  $\text{cm}^{-1}$  appeared after drying of a hematite  
260 layer treated with sulfate at pH 3.6 or with hematite in contact with aqueous sulfate  
261 solutions acidified to below pH 2 with HCl. He suggested that the conversion of aqueous  
262 sulfate to bisulfate occurred during acidification, and thus the peak around 1200  $\text{cm}^{-1}$  was  
263 assigned to the transformation from monodentate to bidentate coordination caused by  
264 drying or to the formation of bisulfate. Sugimoto and Wang (1998) further revealed that  
265 the adsorption mode of sulfate changed from monodentate to bidentate with decreasing  
266 pH and that the bidentate adsorption on {012} and {1m0} surfaces of hematite became  
267 dominant at  $\text{pH} \leq 1.0$ , and they suggested that the enhancement of the peak at 1205  $\text{cm}^{-1}$

268 with direct drying of a wet sample at pH 3.6, found by Hug (1997), seemed to be due to  
269 the pH drop during the drying process. The attribution of the peak at around  $1200\text{ cm}^{-1}$   
270 remains controversial, however, the appearance of this peak undoubtedly reflects the  
271 enhancement of surface acidity. Therefore, in the present study, the increase in the peak  
272 intensity at  $1219\text{ cm}^{-1}$  with the increase of reaction time indicates the increased surface  
273 acidity (Yamaguchi et al., 1986; Persson and Lovgren, 1996; Faguy and Marinković,  
274 1996; Hug, 1997). The slight decrease in intensity of the peak at  $1219\text{ cm}^{-1}$  after it  
275 reaches the maximum may be due to partial dissolution of hematite along with  
276 consumption of surface acidic species, which would lead to the formation of  $\text{Fe}^{3+}$  ions  
277 and some other surface species on the water-containing surface (Chun and Quon, 1973;  
278 Shi et al., 2011).

279 Figure 1b shows typical spectra of the oxidation of  $\text{SO}_2$  on FN-24 recorded as a  
280 function of time in the range of  $1500$  to  $900\text{ cm}^{-1}$ . A prominent peak at  $1158\text{ cm}^{-1}$ , a  
281 shoulder peak at  $1190\text{ cm}^{-1}$  and two weak peaks at  $1080$  and  $987\text{ cm}^{-1}$  are observed in the  
282 spectra. These peaks can be assigned to surface-coordinated sulfate species, that is,  
283 bidentate surface sulfate complex (Zhang et al., 2006; Persson and Lovgren, 1996; Hug,  
284 1997; Peak et al., 1999). Additionally, it is also possible that the feature at  $1190\text{ cm}^{-1}$  is  
285 assigned to bisulfate ( $\text{HSO}_4^-$ ) or sodium sulfate ( $\text{NaSO}_4^-$ ) sorbed as a monodentate  
286 complex on the iron oxide surface, or monodentate sulfate that is hydrogen bonded to an  
287 adjacent surface site (Hug, 1997; Peak et al., 1999). In addition,  $\text{Fe}^{3+}$  ions is present due  
288 to the partial dissolution of hematite in the water-containing acidic surface during the  
289 reaction (Chun and Quon, 1973; Shi et al., 2011), and an iron (III) bisulfate complex ( $\text{Fe}-$   
290  $\text{HSO}_4^{2+}$ ) can also potentially explain the observed feature at  $1190\text{ cm}^{-1}$  (Peak et al., 1999).

291 These results indicated that SO<sub>2</sub> can also be oxidized to sulfate on the surface of the  
292 hematite-nitrate mixture. The spectrum lineshapes are different from those of hematite,  
293 and the most apparent FTIR feature corresponding to the increase of surface product on  
294 FN-24 is the rapidly growing peak at 1158 cm<sup>-1</sup>, indicating that the adsorbed sulfate is the  
295 dominant oxidation product. Therefore, NO<sub>3</sub><sup>-</sup> ions in the nitrate-hematite mixture promote  
296 the heterogeneous uptake of SO<sub>2</sub> and impact the formation of surface species and the  
297 adsorption mode of the formed surface species. A spectral peak-fitting program using  
298 mixed Gaussian-Lorentzian peak fitting is employed to fit peaks to the last spectrum in  
299 Fig. 1b. As shown in Fig. 2, the region from 1400 to 900 cm<sup>-1</sup> is composed of three major  
300 peaks at 1207, 1155 and 1094 cm<sup>-1</sup>, respectively. A very weak peak at 986 cm<sup>-1</sup> cannot  
301 even be seen in Fig. 2. The relative intensity of the observed peaks at 1207, 1155, 1094  
302 and 986 cm<sup>-1</sup> is approximately 5.6:16.1:2.2:0.1, respectively. The presence of the peak at  
303 1207 cm<sup>-1</sup> indicates that the FN-24 surface after the experiment is still acidic. Moreover,  
304 compared with that of the hematite-only substrate (see Section S6 in the Supplement),  
305 weak absorption peaks at 1080, 1050 and 966 cm<sup>-1</sup> appear in the initial stage of  
306 heterogeneous conversion of SO<sub>2</sub> and then gradually disappear or are not easily observed  
307 with increased exposure time. These peaks should be assigned to the stretching motion of  
308 adsorbed sulfite and/or bisulfite (Zhang et al., 2006). The changes in intensity of these  
309 weak absorption peaks implies that the formation of SO<sub>3</sub><sup>2-</sup> and/or HSO<sub>3</sub><sup>-</sup> and their  
310 subsequently rapid consumption on the particle surface. The rapidly growing peak at  
311 1158 cm<sup>-1</sup> as the reaction proceeds also suggests that SO<sub>3</sub><sup>2-</sup> and HSO<sub>3</sub><sup>-</sup> are further  
312 oxidized in the presence of nitrate and less SO<sub>3</sub><sup>2-</sup> and HSO<sub>3</sub><sup>-</sup> are left when compared with  
313 that of hematite-only substrate.

### 314 3.1.2 Surface nitrogen-containing species

315 It should be noted that, compared to the peaks of the formed surface-adsorbed sulfate,  
316 some very low intensity signals appear in the region of 3800 to 1350  $\text{cm}^{-1}$  during the  
317 same experiment with FN-24 (also see Fig. S5 in the Supplement). Figure 3 shows  
318 DRIFTS spectra following  $\text{SO}_2$  uptake on FN-24 particles as a function of reaction time  
319 in this region. Negative peaks at 1599, 1587 and 1567  $\text{cm}^{-1}$  decrease in intensity with  
320 increased exposure time. These peaks are assigned to bridging, bidentate and  
321 monodentate nitrate, respectively (Hixson et al., 2011; Underwood et al., 1999). This  
322 indicates the loss of adsorbed nitrate on FN-24 and suggests that nitrate not only  
323 participates in the heterogeneous conversion of  $\text{SO}_2$  on FN-24 but also have been  
324 consumed during the reaction. This result is consistent with the formation of nitrogen-  
325 containing species such as  $\text{N}_2\text{O}$  and HONO (discussed later in Sect. 3.4). However, it  
326 should be pointed out that the amount of the decay of nitrate is small during the reaction,  
327 which also results in small amounts of  $\text{N}_2\text{O}$  and HONO.

328 Several weak peaks in the 1535-1440  $\text{cm}^{-1}$  region grow with increasing exposure time.  
329 These peaks can be assigned to adsorbed nitrite. The peaks at 1506 and 1487  $\text{cm}^{-1}$  are  
330 assigned to the  $\nu_3$  mode of bridging nitro-nitrito  $\text{NO}_2^-$  and the  $\nu_3$  mode of bridging  
331 monodentate nitrito  $\text{NO}_2^-$  respectively, suggesting the formation of very small amounts of  
332 nitrite (Hixson et al., 2011).

333 Molecularly adsorbed nitric acid and different nitric acid-water complexes,  
334 characterized by the peaks at 1716, 1697, 1686 and 1676  $\text{cm}^{-1}$  (McCurdy et al., 2002;  
335 Ramazan et al., 2006; Finlayson-Pitts et al., 2003), are also observed. These peaks are

336 ascribed to the  $\nu_2$  mode of the asymmetric  $\text{NO}_2$  stretch in nitric acid (monomer or when  
337 complexed to water or another  $\text{HNO}_3$ ) (McCurdy et al., 2002; Ramazan et al., 2006;  
338 Finlayson-Pitts et al., 2003), and the peaks at 1716, 1697, 1686 and  $1676\text{ cm}^{-1}$  are due to  
339  $\text{HNO}_3(\text{H}_2\text{O})_n$ ,  $\text{HNO}_3\text{H}_2\text{O}$ ,  $(\text{HNO}_3)_2$  and  $\text{HNO}_3(\text{H}_2\text{O})_2$  on the surface, respectively.  
340 These peaks increase in intensity with increased exposure time. This result confirms that  
341 adsorbed  $\text{HNO}_3$  is formed from the combination of surface  $\text{H}^+$  with  $\text{NO}_3^-$  as the reaction  
342 proceeds. The formation of  $\text{HNO}_3\text{-H}_2\text{O}$  complexes indicates that nitric acid is stabilized  
343 by water on the particle surface (McCurdy et al., 2002; Ramazan et al., 2006; Finlayson-  
344 Pitts et al., 2003). As a result, no gas phase  $\text{HNO}_3$  was observed in White cell-FTIR  
345 experiments as discussed later. Compared to the assignments of molecularly adsorbed  
346 nitric acid, molecular nitric acid complexed to water and complexed to  $\text{HNO}_3$  itself in  
347 previous reports, these peaks have blue shifted by about  $6\text{ cm}^{-1}$  (McCurdy et al., 2002;  
348 Ramazan et al., 2006), indicating that the asymmetric  $\text{NO}_2$  stretch in nitric acid may be  
349 affected by some other interaction, and the interaction may result in the distortion of the  
350 molecular symmetry of these complexes (Peak et al., 1999).

351 Two weak shoulder peaks at  $1746$  and  $1732\text{ cm}^{-1}$  are seen to grow as the surface is  
352 exposed to  $\text{SO}_2$ . These two peaks should be attributed to the asymmetric  $\nu_a(\text{NO}_2)$  stretch  
353 of  $\text{N}_2\text{O}_4$  adsorbed on the surface, indicating the formation of adsorbed  $\text{N}_2\text{O}_4$  (Goodman et  
354 al., 1999; Finlayson-Pitts et al., 2003). These peaks overlap with those of adsorbed  $\text{HNO}_3$   
355 and increase in intensity with the amount of adsorbed nitric acid on the surface. As  
356 previously reported,  $\text{N}_2\text{O}_4$  can interact with  $\text{HNO}_3$  and/or  $\text{HNO}_3\text{-H}_2\text{O}$  water complexes on  
357 particle surface through hydrogen bonds, in addition to the interactions with  $\text{H}_2\text{O}$   
358 (Finlayson-Pitts et al., 2003). This further indicates that the formed  $\text{N}_2\text{O}_4$  may be held on



359 particle surface with nitric acid and H<sub>2</sub>O present. This is consistent with the fact that no  
360 gas phase N<sub>2</sub>O<sub>4</sub> was detected in White cell-FTIR experiments as discussed later. Surface  
361 N<sub>2</sub>O<sub>4</sub>, which can oxidize many organic and inorganic compounds, was observed as the  
362 crucial oxidant for the oxidation of surface sulfite (Liu et al., 2012). Therefore, the  
363 presence of a very small amount of N<sub>2</sub>O<sub>4</sub> on particle surface may contribute to the  
364 oxidation of surface sulfite and the formation of sulfate and adsorbed nitrite.

### 365 **3.1.3 Surface hydroxyl groups**

366 Two negative absorption peaks are observed at 3661 and 3631 cm<sup>-1</sup> and grow in intensity  
367 as the reaction proceeds. These negative peaks have been previously reported and  
368 attributed to the loss of OH groups from the surface. The peaks at 3661 and 3631 cm<sup>-1</sup> are  
369 stretching vibration modes of isolated surface hydroxyl groups bonded to the surface iron  
370 ions of octahedral sites and tetrahedral sites, respectively (Watanabe et al., 1994), which  
371 implies that surface OH groups are involved in the reaction and are reaction active sites  
372 for SO<sub>2</sub> (Goodman et al., 2001). Pure hematite shows similar absorption. Another weak  
373 broad absorption peak extending from 3500 to 2520 cm<sup>-1</sup> slowly increases in intensity  
374 with the increase of reaction time. This broad peak is primarily associated with O-H  
375 vibration of hydrogen-bonded OH groups of acid and should be assigned to molecular  
376 nitric acid complexed to water or to some extent complexed to HNO<sub>3</sub> itself (Börensén et  
377 al., 2000; Goodman, et al., 1999; Ramazan et al., 2006; Finlayson-Pitts et al., 2003),  
378 which is consistent with the formation of surface-adsorbed HNO<sub>3</sub> discussed earlier.

379 Overall, the results indicate that nitrate participates in the heterogeneous reactions of  
380 SO<sub>2</sub>, changes the conversion pathway of SO<sub>2</sub> and the formation rate of sulfate, and leads

381 to the formation of surface  $\text{HNO}_3$ ,  $\text{N}_2\text{O}_4$  and  $\text{NO}_2^-$  species. A summary of the assignments  
382 for the surface species peaks observed in this study based on frequencies reported in  
383 earlier studies is given in Table 1.

### 384 **3.2 Effect of nitrate on the rate of sulfate formation and uptake coefficient for $\text{SO}_2$** 385 **on hematite-nitrate mixture at 298 K**

386 The formation rates of sulfate on different samples were investigated. All of the DRIFTS  
387 experiments were performed at 298 K with 30 mg of sample, and the amount of sulfate  
388 on each sample after DRIFTS experiment was determined by ion chromatography to  
389 quantify the sulfate formation rate  $d[\text{SO}_4^{2-}]/dt$ . It is found that over a large concentration  
390 range the integrated sulfate absorption ( $1000\text{ cm}^{-1}$  to  $1400\text{ cm}^{-1}$ ) is proportional to the  
391 sulfate concentration. The formation rate is therefore translated from the integrated  
392 sulfate absorbance of the spectrum to the total number of sulfate ions on the sample after  
393 the reaction by a conversion factor. The conversion factor is obtained from a calibration  
394 plot with integrated sulfate absorption vs. number of sulfate ions formed at the end of an  
395 experiment, and a value of  $f = 2.58 \times 10^{18}$  ( $\text{ions g}^{-1}$  integrated absorption units $^{-1}$ ) is  
396 calculated. Since the absorption peaks of different reaction product species overlap one  
397 another, the peaks were deconvoluted before integration in some experiments.

398 The gas-phase concentrations of the reactive gases in a continuous flow were kept  
399 constant during the DRIFTS experiments and since  $\text{O}_2$  was in great excess compared to  
400  $\text{SO}_2$ , the concentration of  $\text{O}_2$  could be regarded as constant. The number of sulfate ions  
401 formed at the initial stage of reaction is generally considered to be small relative to the  
402 number of reactive surface sites, and thus the latter at initial stage can be assumed to be

403 constant (B örensen, et al., 2000). Therefore, the reaction order can be determined from a  
 404 bilogarithmic plot of initial rate of sulfate formation ( $\log(d[\text{SO}_4^{2-}]/dt)$ ) vs. the  
 405 concentration of  $\text{SO}_2$  ( $\log[\text{SO}_2]$ ), as previously reported (B örensen et al., 2000; Wu et al.,  
 406 2011). For this purpose, the experiments with different  $\text{SO}_2$  concentrations were  
 407 performed, and the sulfate formation rate  $d[\text{SO}_4^{2-}]/dt$  was obtained from the slope of the  
 408 initial linear portion (0-60 min) in the curve of sulfate formation as a function of time. No  
 409 saturation effects on sulfate formation were observed. For the mixture such as FN-24  
 410 used in this study, the plot gave a slope of  $1.09 \pm 0.10$  ( $2\sigma$ ), which indicates a reaction  
 411 order of 1 for  $\text{SO}_2$ . The reaction order with respect to  $\text{SO}_2$  was also examined from White  
 412 cell-FTIR experimental data by examining the rates of  $\text{SO}_2$  decay. The calculated result is  
 413 consistent with that using DRIFTS data (correlation coefficient of  $\ln[\text{SO}_2]_0/[\text{SO}_2]$  vs. time  
 414 (t) was greater than 0.99). That is, the heterogeneous oxidation of  $\text{SO}_2$  on the hematite-  
 415 nitrate mixture was still a pseudo-first-order reaction.

416 The reactive uptake coefficient ( $\gamma$ ) is defined as the rate of sulfate formation on the  
 417 surface ( $d[\text{SO}_4^{2-}]/dt$ ) divided by the total number of surface collisions per unit time ( $Z$ ).

$$418 \quad \gamma = \frac{d[\text{SO}_4^{2-}]/dt}{Z} \quad (1)$$

$$419 \quad Z = \frac{1}{4} \times A_s \times [\text{SO}_2] \times v \quad (2)$$

$$420 \quad v = \sqrt{8RT / \pi M_{\text{SO}_2}} \quad (3)$$

421 where  $v$  is the mean molecular velocity of  $\text{SO}_2$ ,  $A_s$  is the effective sample surface,  $R$  is  
 422 the gas constant,  $T$  is the temperature and  $M_{\text{SO}_2}$  is the molecular weight of  $\text{SO}_2$  (Ullerstam,

423 et al., 2003). Two extreme cases of effective sample surface are usually considered for  
424 calculating the uptake coefficient (Ullerstam et al., 2002). If the reaction probability is  
425 high, the reactants would have no time to diffuse into the sample before reacting and the  
426 effective surface area will be the geometric surface area of the sample holder ( $A_{\text{geometric}}$ ).  
427 If the reaction probability is low, the reactants may have enough time to diffuse into the  
428 entire sample and thus the BET surface area ( $A_{\text{BET}}$ ) would more appropriately represent  
429 the effective area. Therefore, upper and lower limits of uptake coefficients can be  
430 calculated using the geometric and BET surface area as the reactive surface area,  
431 respectively (denoted as  $\gamma_{\text{geometric}}$  and  $\gamma_{\text{BET}}$ , respectively).

432 Table 2 shows the sulfate formation rates and the two kinds of uptake coefficients of  
433  $\text{SO}_2$  on hematite and the hematite-nitrate mixtures at 298 K. The sulfate formation rate  
434 and the two kinds of uptake coefficients first increase and then decrease with increasing  
435 mass fraction of nitrate, and no sulfate formation is observed on pure sodium nitrate. For  
436 mixtures, the FN-24 sample presents the highest sulfate formation rate. Correspondingly,  
437 the FN-24 sample shows the highest  $\gamma_{\text{geometric}}$ , and its  $\gamma_{\text{geometric}}$  is about 5.5 times higher  
438 than that of hematite alone. Although the sulfate formation rate for FN-24 is higher than  
439 that for FN-48, the BET uptake coefficient  $\gamma_{\text{BET}}$  for FN-24 is less than that for FN-48.  
440 This is mainly because that the FN-48 has smaller BET surface area than the FN-24, and  
441 hence the FN-48 presents the highest  $\gamma_{\text{BET}}$ . Its  $\gamma_{\text{BET}}$  is about 8 times higher than that of  
442 pure hematite. Therefore, the reaction behavior of  $\text{SO}_2$  adsorbed on hematite is altered by  
443 the availability of nitrate. An appropriate amount of nitrate greatly enhances the reactivity  
444 of the hematite-nitrate mixtures and favors the formation of sulfate on hematite. The  
445 promotion effect of a low to moderate amount of nitrate should receive close attention

446 because the nitrate content is close to that in ambient particles (Ho et al., 2003), and this  
447 effect may help to predict the formation of sulfate aerosols in the atmosphere.

### 448 **3.3 Effect of nitrate on heterogeneous reactivity of SO<sub>2</sub> on hematite at 298 K**

449 The White cell-FTIR can be used to trace gaseous reactants and possible gaseous  
450 products formed from the heterogeneous reaction of SO<sub>2</sub>, but it cannot be used to observe  
451 surface species formed on the sample surface. In situ White cell-FTIR spectra collected  
452 from exposure of the FN-24 sample to 50 ppm of SO<sub>2</sub> at room temperature are shown in  
453 Fig. 4. The strong absorption peaks at 1373, 1360, and 1348 cm<sup>-1</sup> and the weak ones at  
454 1163 and 1135 cm<sup>-1</sup> are readily observed in the spectra. These peaks are assigned to the  
455 characteristic peaks of gaseous SO<sub>2</sub> (Fu et al., 2007; Zhang et al., 2006). The intensities  
456 of these peaks in the spectra decrease rapidly as the reaction proceeds, indicating that the  
457 concentration of SO<sub>2</sub> decreases while it reacts on the surface of FN-24. The other FN  
458 series and pure hematite samples upon exposure to 50 ppm of SO<sub>2</sub> at room temperature  
459 show similar absorption but different rates of SO<sub>2</sub> consumption, revealing that the sample  
460 reactivity varies with mass fractions of sodium nitrate. No uptake of SO<sub>2</sub> is observed on  
461 the pure sodium nitrate. The results indicate that the reactivity increases first and then  
462 decreases with increasing mass fraction of sodium nitrate in the samples. This is  
463 consistent with that observed in DRIFTS experiments.

### 464 **3.4 Effect of nitrate on gas-phase products from the heterogeneous uptake of SO<sub>2</sub> on** 465 **hematite**

466 It is worth noting that several absorption peaks of gaseous HONO appear in the spectra in  
467 the White cell-FTIR experiment by exposing the FN series samples to lower

468 concentrations of SO<sub>2</sub>. Although adsorbed HNO<sub>3</sub> has been detected during the DRIFTS  
469 experiments, gas phase nitric acid has not been observed in White cell-FTIR experiments,  
470 suggesting that molecular nitric acid is firmly adsorbed on the particle surface in the  
471 presence of water. Figure 5 shows the representative in situ FTIR spectra collected from  
472 exposure of the FN-90 sample to 12.5 ppm of SO<sub>2</sub> for different times. A difference  
473 spectrum shown in Fig. 5e was obtained by subtracting the spectrum in Fig. 5c from that  
474 in Fig. 5d. As shown in Fig. 5, there are no absorption peaks of gas-phase HONO before  
475 430 min but several weak HONO absorption peaks centered at 1262, 850 and 790 cm<sup>-1</sup>  
476 are observed when the reaction time is prolonged to 1170 min (Fig. 5d) (Wingen et al.,  
477 2000). The difference spectrum shown in Fig. 5e further confirms the existence of HONO,  
478 revealing that a trace amount of gaseous HONO is formed during the reaction of SO<sub>2</sub> on  
479 the hematite-nitrate mixture. To the best of our knowledge, this is the first observation of  
480 the formation of HONO in such a nitrate-containing reaction system. Observation of  
481 HONO formation is of particular significance because it plays an important role in the  
482 degradation of primary and secondary atmospheric pollutants by serving as a major  
483 source of hydroxyl radicals. HONO formed from heterogeneous reaction of nitrogen  
484 dioxide has been extensively studied on different materials like mineral dust particles and  
485 soot (Finlayson-Pitts et al., 2003; Arens et al., 2001), and HONO is known to be in  
486 equilibrium with NO and NO<sub>2</sub> in the gas phase via its self-reaction (Pitts et al., 1984).  
487 However, the heterogeneous reaction of nitrogen dioxide and the self-reaction of HONO  
488 may be negligible in our system because no absorption peaks of gas-phase NO and NO<sub>2</sub>  
489 in the spectral range from 1200 to 1900 cm<sup>-1</sup> are observed. It is possible that gaseous NO  
490 and NO<sub>2</sub> are present at concentrations below detection limits. But on the other hand, the

491 weak absorption peaks of HONO may suggest the very low HONO partial pressure, and  
492 hence the self-reaction of HONO is probably not relevant at such a low HONO pressure.

493 The result also suggests that the initial surface-formed HONO may be simultaneously  
494 consumed by some secondary reactions in this system. On the one hand, no absorption  
495 peaks of HONO by exposing the FN series samples to 50 ppm SO<sub>2</sub> for the same reaction  
496 time were observed. This fact suggests that the possible consumption reactions of HONO  
497 may be the ones between HONO and the surface abundant reduced S(IV) species, such as  
498 sorbed or surface-coordinated H<sub>2</sub>SO<sub>3</sub>, HSO<sub>3</sub><sup>-</sup> and SO<sub>3</sub><sup>2-</sup> species, which led to gaseous  
499 HONO levels below detection limits before the complete consumption of these species.  
500 On the other hand, the high concentration of SO<sub>2</sub> means that there are much more  
501 reduced S(IV) species existing on the sample surface than those formed from the low  
502 concentration of SO<sub>2</sub>. This also implies that HONO will be observed within a long  
503 reaction time if the high concentration of SO<sub>2</sub> is used. An earlier study of Martin *et al.*  
504 observed that S(IV) species can be rapidly oxidized to sulfate by HONO in acidic  
505 aqueous aerosols (Martin et al., 1981), which would support the secondary reactions of  
506 HONO with S(IV) species in our experiments and reveal the potential role of HONO in  
507 the heterogeneous conversion of SO<sub>2</sub>. In addition, the absorption peaks between 1400 and  
508 1800 cm<sup>-1</sup> are mainly attributed to H<sub>2</sub>O molecule vibrations. These absorption peaks  
509 gradually grow in intensity with the increase of reaction time because H<sub>2</sub>O molecules can  
510 evaporate slowly from the humid surface of FN samples placed in the White cell.

511 Rivera-Figueroa et al. found that the reaction between HNO<sub>3</sub> and SO<sub>2</sub> on silica  
512 surfaces in the presence of water films does not occur (Rivera-Figueroa et al., 2003).  
513 Martin and co-workers also reported that nitric acid in solution does not react with

514 dissolved SO<sub>2</sub> (Martin et al., 1981). Furthermore, in our study the experiments in which  
515 humid pure nitrate was exposed to SO<sub>2</sub> using White cell-FTIR and DRIFTS techniques  
516 also show no detectable gas phase products, indicating that pure nitrate cannot interact  
517 with SO<sub>2</sub>. Therefore, considering the species in the reaction systems mentioned above,  
518 these previous studies indicate that the reactions between HNO<sub>3</sub> and S(IV) species cannot  
519 occur. Moreover, reductive dissolution of Fe (III) oxides and reduction of Fe (III) by  
520 sulfite have been suggested as possible sources of Fe (II) (Behra and Sigg, 1990), and  
521 the formation of Fe<sup>2+</sup> via heterogeneous reaction of SO<sub>2</sub> oxidation on the surface of Fe<sub>2</sub>O<sub>3</sub>  
522 has already been verified by measuring the amount of Fe<sup>2+</sup> during the reaction (Zhang et  
523 al., 2007; Ansari et al., 1997). Therefore, among the possible surface species in our  
524 reaction system, Fe<sup>2+</sup> is the only reduced species that can react with NO<sub>3</sub><sup>-</sup> in the presence  
525 of H<sup>+</sup>. In other words, the only formation pathway of HONO is the reduction of NO<sub>3</sub><sup>-</sup> by  
526 the reductive Fe<sup>2+</sup> in the presence of H<sup>+</sup>, while the reductant Fe<sup>2+</sup> can be fed from the  
527 recycle from the reduction of Fe<sup>3+</sup> by dissolved SO<sub>2</sub>. HONO formation processes in the  
528 atmosphere are still under discussion, especially during daytime where large  
529 discrepancies are found between mixing ratios calculated from known gas phase  
530 chemistry and measured daytime mixing ratios (Kleffmann et al., 2005). Our results also  
531 suggest that the heterogeneous reaction of SO<sub>2</sub> on nitrate-containing hematite may serve  
532 as a potential source for HONO, which may have implications on the oxidant chemistry  
533 in the atmosphere. However, the low yield of gaseous HONO may suggest that the  
534 contribution of HONO by this pathway to the atmospheric gas phase HONO may be  
535 negligible, but the formation of unreleased HONO in the particles may be significant for  
536 the conversion of SO<sub>2</sub> and the formation of sulfate in the atmosphere.



537 In addition, it is interesting to note that N<sub>2</sub>O is formed in the process of the  
538 heterogeneous uptake of SO<sub>2</sub> on the hematite-nitrate mixtures at both low and high SO<sub>2</sub>  
539 concentrations. As shown in Fig. 5, two N<sub>2</sub>O absorption peaks at 2235 and 2208 cm<sup>-1</sup>  
540 appear and slowly grow in intensity with the increase of reaction time (Hussain and  
541 Rahman, 2006), indicating that gas-phase N<sub>2</sub>O is produced in the FT-IR experiments. The  
542 concentration of N<sub>2</sub>O gradually increases and approaches a constant (ca. 418 ppb) as the  
543 reaction proceeds (see Fig. 5f). The gas-phase concentrations of N<sub>2</sub>O are determined  
544 according to a linear relationship between the integrated area of the gaseous N<sub>2</sub>O  
545 absorption peaks in the range 2258-2160 cm<sup>-1</sup> and its concentration ( $r^2 = 0.996$ ). The  
546 linear relationship is obtained using in situ White cell-FTIR and different concentrations  
547 of N<sub>2</sub>O standard gas. The observed formation of N<sub>2</sub>O is of particular importance because  
548 it is an extremely influential greenhouse gas and directly involved in global warming as  
549 well as in the destruction of ozone in the stratosphere. It has been reported that sulfur (IV)  
550 species such as H<sub>2</sub>SO<sub>3</sub> can be easily oxidized by HONO at low pH (0.6-3.2) and the gas  
551 phase product is N<sub>2</sub>O (Martin et al., 1981). Therefore, it is reasonable to speculate that  
552 N<sub>2</sub>O is formed from the reduction of HONO by S(IV) species such as sorbed or surface-  
553 coordinated H<sub>2</sub>SO<sub>3</sub>, HSO<sub>3</sub><sup>-</sup> and SO<sub>3</sub><sup>2-</sup> species on the mixture sample surface before  
554 HONO is released (Pires et al., 1996; Pires et al., 1997). This observation provides  
555 evidence for the formation of nitrous oxide from the hematite-nitrate mixtures at ambient  
556 temperature, and suggests a new potential atmospheric source of N<sub>2</sub>O. This source is  
557 currently not accounted for in the global N<sub>2</sub>O budget. The result may help to explain why  
558 the sources of N<sub>2</sub>O exceed the estimated sinks in the atmosphere and the observed  
559 increase in atmospheric N<sub>2</sub>O. However, it should be pointed out that the high surface to

560 volume ratio of the experiments may lead to relatively more N<sub>2</sub>O than in the atmosphere.  
561 Meanwhile the lifetime of HONO in the atmosphere is probably limited by photolysis.  
562 The relative importance of this source needs further study.

563 To further confirm the formation of HONO and N<sub>2</sub>O, we also performed heterogeneous  
564 reactions of SO<sub>2</sub> (50 ppm) on humid hematite, FN-24 and FN-90 in the presence of O<sub>2</sub>  
565 (21% v/v) in three brown glass bottles in the dark for 3-7 days. The dark condition is  
566 selected to avoid the photolysis of HONO and the photochemistry of adsorbed nitrate  
567 (Schuttlefield et al., 2008). The selected long reaction time favors the release of the  
568 produced HONO and the accumulation of N<sub>2</sub>O. Figure 6 shows the digital photos of the  
569 three samples after reaction with SO<sub>2</sub> in the dark at room temperature for about 7 days.  
570 Interestingly, the heterogeneous reactions of SO<sub>2</sub> on the surfaces of FN-24 and FN-90  
571 present unique phenomena, and some liquid drops cover the interior walls of glass bottles,  
572 which is different from that presented by the reaction of SO<sub>2</sub> on the pure hematite. The  
573 latter does not show the similar phenomenon. The liquid drops show strong acidity which  
574 has been measured with pH test paper (the pH was about 1). Ion chromatography analysis  
575 shows that the liquid drops mainly contain sulfate ions while the concentration of nitrate  
576 ion is below the detection limit. These results indicate that the liquid drop is sulfuric acid.  
577 The appearance of the liquid drops should be attributed to the presence of gas phase  
578 HONO. Gas phase HONO transforms SO<sub>2</sub> that is present in the gas-phase or adsorbed on  
579 the bottle walls into sulfuric acid, while reactive HONO is produced from the  
580 heterogeneous reaction of SO<sub>2</sub> on the surface of the hematite-nitrate mixture and the  
581 subsequent release. The HONO vapor adsorbs onto the interior wall of the glass bottle,  
582 and together with H<sub>2</sub>O initiates the oxidation of SO<sub>2</sub> and the subsequent formation of

583 H<sub>2</sub>SO<sub>4</sub>. Additionally, the gas-phase species in the three glass bottles were analyzed by  
584 using SPMS/GC-MS technique, and N<sub>2</sub>O is only found from the reactions of SO<sub>2</sub> on FN-  
585 24 and FN-90, no NO, NO<sub>2</sub> and N<sub>2</sub>O<sub>4</sub> are detected (see Fig. S6 in the Supplement).  
586 Therefore, considering the experimental results mentioned above, the formation of  
587 HONO and N<sub>2</sub>O during the reaction of SO<sub>2</sub> on the hematite-nitrate mixture has been  
588 further verified by this experiment, which is consistent with the observations from in situ  
589 White Cell-FTIR experiments. This experiment also verifies that N<sub>2</sub>O and HONO can be  
590 produced from the reaction of SO<sub>2</sub> on the hematite-sodium nitrate mixtures not only in  
591 daytime but also at night. Although the concentration of the formed HONO cannot be  
592 accurately measured during the process of the heterogeneous uptake of SO<sub>2</sub> on the  
593 hematite-nitrate mixture because the formed HONO is being continuously consumed on  
594 the particle surface, it may be important not only in daytime but also at night for the  
595 conversion of atmospheric SO<sub>2</sub> and the formation of atmospheric sulfate. Such aspects  
596 should be further explored in future studies.

### 597 **3.5 Effect of nitrate on the morphology of surface product formed from the uptake** 598 **of SO<sub>2</sub> onto hematite**

599 Scanning electron micrographs of sample particles before and after reaction with gaseous  
600 SO<sub>2</sub> were obtained from a Philips XL-30 scanning electron microscope equipped with an  
601 energy dispersive X-ray spectrometer (SEM-EDX). Figure 7 shows SEM images of FN-  
602 24 and FN-90 particles before (Fig. 7a and c) and after (Fig. 7b and d) exposure to  
603 gaseous SO<sub>2</sub> in the DRIFTS experiments. The two unreacted samples show the  
604 morphology of aggregated particles and consist of primary particles with an averaged  
605 particle size of over 100 nm. After the reaction with SO<sub>2</sub>, there are some flaky substances

606 covering some particle surfaces. EDX analysis shows that the flaky substance is  
607 composed of 57.89% O, 11.70% Na, 11.48% S and 18.93% Fe (Fig. 7e). The  
608 characteristic peaks in the EDX spectrum indicates that no nitrogen is detected on the  
609 flaky substance, indicating the formation of sulfate on the particle surface and the change  
610 in particle morphology. This result should be attributed to the enhanced formation of  
611 sulfate on the hematite surface due to the presence of nitrate. It should be noted that we  
612 cannot observe a similar phenomenon on the pure hematite after exposure to SO<sub>2</sub>.

### 613 **3.6 Role of surface adsorbed water under the influence of nitrate**

614 Previous studies indicate that surface-adsorbed water plays an important role in the  
615 heterogeneous chemistry of atmospheric SO<sub>2</sub> (Nanayakkara et al., 2012). However, little  
616 is known about the role of surface-adsorbed water in the heterogeneous oxidation of SO<sub>2</sub>  
617 on hematite-nitrate mixture. Therefore, the role of surface-adsorbed water in the  
618 heterogeneous oxidation of SO<sub>2</sub> on FN-24 was further investigated using in situ DRIFTS.  
619 In order to prevent the sample particles from being brought out from the in situ chamber,  
620 a vacuum wasn't applied during these experiments. The sample was first pretreated at  
621 preset temperature for 60 min in a stream of Ar in a total flow of 100 mL min<sup>-1</sup>. The  
622 preset temperatures were 298, 303, 373, 423, 473 and 573 K, respectively. After 60 min  
623 the heated sample in the reaction chamber was cooled to 298 K under Ar flow, and a  
624 background spectrum of the unreacted powder sample was collected. Subsequently, IR  
625 spectra were collected as a function of reaction time after being exposed to gaseous  
626 reactants. The results are shown in Fig. 8. The pre-treated sample at 373, 423 and 473 K  
627 enhances the reactivity of hematite, and the sulfate formation rates at 373 and 423 K  
628 increase by a factor of 1.28 and 1.25 compared with that at 298 K, respectively,

629 indicating that the presence of appropriate amount of water on particle surface will favor  
630 the heterogeneous conversion of SO<sub>2</sub>. However, with a further increase in pre-treated  
631 temperature the reactivity decreases, and the sample pre-treated at 573 K shows even  
632 lower reactivity than that at 298 K. Pre-treatment of the sample is known to mainly  
633 remove surface- adsorbed water, and, at higher temperature, surface dehydration occurs.  
634 The observed increases in the reactivity of the sample pre-treated at 373 and 423 K are  
635 due to the partly removal of physisorbed water, which may serve as an inhibitor for the  
636 SO<sub>2</sub> oxidation by blocking access to the active sites. Samples pre-treated at higher  
637 temperatures (573 K) displays removal of the physisorbed water along with partly  
638 desorption of surface hydroxyl groups (Egashira et al., 1981), resulting in a decrease in  
639 the sample reactivity. In agreement with other studies, surface hydroxyl groups can be the  
640 active sites for the conversion of SO<sub>2</sub>.

### 641 **3.7 Proposed mechanism of SO<sub>2</sub> uptake on hematite-nitrate mixtures**

642 On the basis of the experimental observations described above, a reaction mechanism for  
643 the heterogeneous reaction of SO<sub>2</sub> on the hematite-nitrate mixture is proposed. Previous  
644 studies have shown that nitrate ions can be readily solvated by adsorbed water molecules  
645 under ambient conditions due to their hygroscopic nature (Hoffman et al., 2004), and thus  
646 nitrate in mixture sample will make more water molecules be adsorbed on the particles  
647 when the prepared mixture sample is kept in a desiccator at 68% RH for 48 h, and leads  
648 to weak water loss during the purge and subsequent reaction processes. The adsorbed  
649 water will favor the uptake of SO<sub>2</sub> and the formation of S(IV) species (Zhang et al., 2007;  
650 Preszler Prince et al., 2007). Therefore, in the initial stage of heterogeneous conversion of

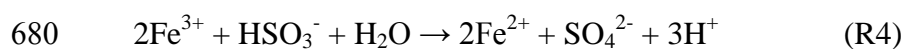
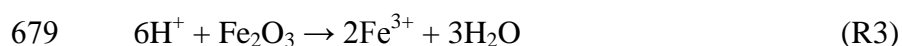
651 SO<sub>2</sub> on the nitrate-hematite mixture, the following reactions will occur (Zhang et al.,  
652 2007):



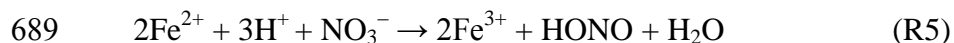
655 Earlier studies of SO<sub>2</sub> adsorption on metal oxides have shown that Lewis acid sites,  
656 hydroxyl groups and oxygen vacancies can all play a role in the surface chemistry  
657 (Goodman et al., 2001; Fu et al., 2007; Baltrusaitis et al., 2007, 2010). Surface hydroxyl  
658 groups are involved in the adsorption of sulfur dioxide, and in particular, sulfur dioxide  
659 reacts with either one surface O–H group to yield adsorbed bisulfite or two surface O–H  
660 groups to yield adsorbed sulfite and water. In the current study, the used nitrate-hematite  
661 mixtures are still loose fine powders after they are saturated at 68% RH for 48 h, and  
662 there may be several water molecule layers resisting on humid sample surfaces. Therefore,  
663 surface sulfate and/or bisulfate can also be produced on the nitrate-hematite mixture  
664 particles through surface active oxygen and hydroxyl, while the active oxygen and  
665 hydroxyl can be formed from the interaction of O<sub>2</sub> and H<sub>2</sub>O with the surface of hematite  
666 (Baltrusaitis et al., 2007). The formation mechanism of the surface sulfate and/or  
667 bisulfate during initial reaction stages should also be the same as that reported previously  
668 (Goodman et al., 2001; Baltrusaitis et al., 2007; Fu et al., 2007; Zhang et al., 2007). That  
669 is, the gaseous SO<sub>2</sub> reacts with surface active oxygen and hydroxyl to form surface S(IV)  
670 species (i.e. adsorbed sulfur species and surface-coordinated HSO<sub>3</sub><sup>-</sup> and SO<sub>3</sub><sup>2-</sup>), and then  
671 these S(IV) species are further oxidized to surface S (VI) species including SO<sub>4</sub><sup>2-</sup> and/or

672 HSO<sub>4</sub><sup>-</sup> in the presence of O<sub>2</sub> and H<sub>2</sub>O (Fu et al., 2007; Zhang et al., 2007; Preszler Prince  
673 et al., 2007).

674 The reactions mentioned above will lead to the formation of an acidic surface. On the  
675 acidic surface, hematite will be partially dissolved to give Fe<sup>3+</sup> ions in the water-rich  
676 surface (Chun and Quon, 1973; Shi et al., 2011), which in turn oxidizes HSO<sub>3</sub><sup>-</sup> to form  
677 SO<sub>4</sub><sup>2-</sup>. As previously reported, Fe<sup>2+</sup> ions are generated during this process (Behra and  
678 Sigg, 1990; Ansari et al., 1997; Zhang et al., 2007).

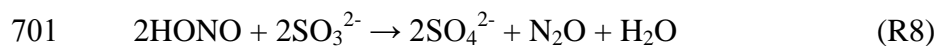


681 It is well established that the nitrate ion is a strong oxidizing agent in highly acidic  
682 solutions that is capable of changing the oxidation state of reduced species (Burley and  
683 Johnston, 1992). As the above reactions proceed, the surface of the mixed hematite-  
684 nitrate sample becomes more acidic, and adsorbed nitric acid and nitric acid-water  
685 complexes are gradually formed on the surface. Once the surface becomes sufficiently  
686 acidified, the interaction between nitric acid and Fe<sup>2+</sup> ion occurs on acidic surface, and  
687 the Fe<sup>2+</sup> ion is oxidized and HONO is produced (Summers, 2005), as given in the  
688 following ionic equation:

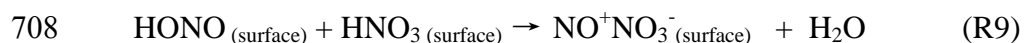


690 The re-generated Fe<sup>3+</sup> further oxidizes the S(IV) species to S(VI) species and produces  
691 Fe<sup>2+</sup> ions. With the cycle of the above reactions, more and more sulfates and HONO are  
692 produced. As shown in previous studies, S(IV) species can be rapidly oxidized to sulfate

693 by HONO, and HONO can be reduced to N<sub>2</sub>O in acidic aqueous aerosols (Martin et al.,  
 694 1981; Pires et al., 1996, 1997). Thus, the formed HONO is also considered to react  
 695 promptly with surface S(IV) species (i.e. sorbed H<sub>2</sub>SO<sub>3</sub>, HSO<sub>3</sub><sup>-</sup> and SO<sub>3</sub><sup>2-</sup>) before it  
 696 escapes to the gas phase, which also results in the formation of N<sub>2</sub>O and more sulfates on  
 697 the particle surface. As reported previously (Martin et al., 1981), the stoichiometry should  
 698 be as follows:



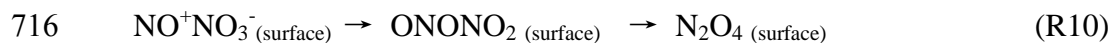
702 An alternate mechanism involving consumption of HONO and formation of sulfate is  
 703 based on that proposed by Finlayson-Pitts et al. (2003) and Liu et al. (2012). That is,  
 704 reaction of the surface formed HONO with HNO<sub>3</sub> on the surface generates NO<sup>+</sup>NO<sub>3</sub><sup>-</sup>.  
 705 This reaction can be thought of as a reaction of NO<sub>3</sub><sup>-</sup> with NO<sup>+</sup> formed from the reaction  
 706 of HONO with the HNO<sub>3</sub>, i.e., the reverse of the overall NO<sub>2</sub> hydrolysis reaction. The  
 707 reaction process may be as follows:



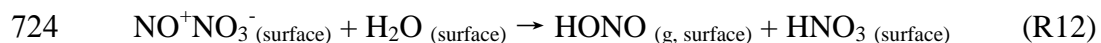
709 Some NO<sup>+</sup>NO<sub>3</sub><sup>-</sup><sub>(surface)</sub> isomerizes to surface asymmetric ONONO<sub>2</sub>, and then ONONO<sub>2</sub>  
 710 converts to small amount of N<sub>2</sub>O<sub>4</sub> (Finlayson-Pitts et al., 2003; Liu et al., 2012). The  
 711 formed N<sub>2</sub>O<sub>4</sub> interacts strongly with water and adsorbed HNO<sub>3</sub> and would be more likely  
 712 present on the surface (Finlayson-Pitts et al., 2003). Some NO<sup>+</sup>NO<sub>3</sub><sup>-</sup><sub>(surface)</sub> oxidizes  
 713 surface S(IV) species to sulfate, while NO<sup>+</sup>NO<sub>3</sub><sup>-</sup> itself is reduced to nitrite (M represents



714 the surface metal sites). This can explain small amounts of N<sub>2</sub>O<sub>4</sub> and nitrite observed in  
715 our study:



718 Once the surface S(IV) species have been completely consumed, the remaining  
719 NO<sup>+</sup>NO<sub>3</sub><sup>-</sup> will react with surface adsorbed water to generate HONO and adsorbed HNO<sub>3</sub>  
720 (Finlayson-Pitts et al., 2003), and subsequently the formed HONO through the reaction of  
721 NO<sup>+</sup>NO<sub>3</sub><sup>-</sup> with water and the unconsumed HONO by S(IV) species will be slowly  
722 released into the gas phase. Accordingly, HONO rather than N<sub>2</sub>O<sub>4</sub> is responsible for the  
723 formation of H<sub>2</sub>SO<sub>4</sub> liquid drops on the interior wall of the glass bottle in the dark.



725 Therefore, the appearance of HONO will favor the oxidation of S(IV) species on the  
726 surface and lead to the formation of more sulfates (Martin et al., 1981). With the cycle of  
727 the above reactions, more and more sulfates and N<sub>2</sub>O are produced. Once the reduced  
728 S(IV) species on the surface have been completely consumed, the remaining and  
729 subsequently formed HONO will slowly escape into the gas phase, and be detected by  
730 FTIR.

731 In addition, it is well-known that N<sub>2</sub>O can be formed during heterogeneous hydrolysis  
732 of gas-phase NO<sub>2</sub> via HONO on acidic oxide surfaces (Finlayson-Pitts et al., 2003;  
733 Wiesen et al., 1995). Therefore, another possibility for the formation of N<sub>2</sub>O is similar to

734 the conversion proposed by Finlayson-Pitts *et al* and Wiesen *et al* (Finlayson-Pitts et al.,  
735 2003; Wiesen et al., 1995). That is, reaction of HONO and its protonated forms ( $\text{H}_2\text{ONO}^+$   
736 or possibly  $\text{NO}^+$ ) generates hyponitrous acid,  $\text{HON}=\text{NOH}$ . The self-reaction of  $(\text{HON})_2$   
737 then decomposes to  $\text{N}_2\text{O}$  under acidic conditions. Similar chemistry has also been  
738 proposed for the formation of  $\text{N}_2\text{O}$  under acidic conditions in the presence of  $\text{SO}_2$  (Pires  
739 et al., 1997).

740 Above all, the consumed nitrate during the reaction will favor the uptake of more  $\text{SO}_2$   
741 molecules and produce more surface sulfate, while secondary chemistry of intermediate  
742 HONO will also result in the formation of gas phase  $\text{N}_2\text{O}$ . Furthermore, more adsorbed or  
743 surface-coordinated S(IV) species produced from higher concentrations of  $\text{SO}_2$  also  
744 indicate that it will take a longer reaction time to observe the formation of gaseous  
745 HONO. The proposed mechanism provides new insights into some unsolved atmospheric  
746 problems such as unknown sources of  $\text{N}_2\text{O}$  and potential HONO, unknown  $\text{SO}_2$  sinks and  
747 unknown sulfate formation pathways in the troposphere, and this chemistry also helps to  
748 explain the discrepancy between model-predicted sulfate and field observations of sulfate  
749 in the atmosphere (Laskin et al., 2003). The reaction mechanism of the heterogeneous  
750 oxidation of  $\text{SO}_2$  on hematite in the presence of nitrate is summarized in Fig. 9.

751

## 752 **4 Conclusions**

753 The effects of nitrate on heterogeneous conversion of  $\text{SO}_2$  on hematite at room  
754 temperature have been investigated. It is found that nitrate participates in the  
755 heterogeneous reactions of  $\text{SO}_2$ , changes the conversion pathway of  $\text{SO}_2$ , and leads to the

756 formation of HNO<sub>3</sub>, N<sub>2</sub>O, HONO and more sulfate, revealing that nitrate has a significant  
757 impact on the heterogeneous conversion of SO<sub>2</sub> to sulfate. The heterogeneous uptake of  
758 SO<sub>2</sub> on hematite is enhanced by a low to moderate amount of nitrate, and more sulfates  
759 are formed on hematite. For mixtures, the sample containing 24% nitrate exhibits the  
760 highest sulfate formation rate, and its corresponding uptake coefficient calculated by  
761 geometric surface area is about 5.5 times higher than that of hematite alone. The sample  
762 containing 48% nitrate presents the highest BET uptake coefficient, and the value is  
763 about 8 times higher than that of pure hematite. The enhanced formation of sulfate on  
764 particle surfaces and the change of particle surfaces would affect the hygroscopicity,  
765 optical properties and lifetime of the particle in the atmosphere. The observed formation  
766 of HONO and N<sub>2</sub>O is of particular importance. The formation of potential HONO by this  
767 pathway may be significant for the conversion of SO<sub>2</sub> and the formation of sulfate in the  
768 atmosphere. The observed formation of N<sub>2</sub>O may help to explain the difference between  
769 the sources of N<sub>2</sub>O and the estimated sinks in the atmosphere and the observed increase  
770 in atmospheric N<sub>2</sub>O. This study not only reveals the effects of nitrate on heterogeneous  
771 conversion of SO<sub>2</sub> on hematite but also provides new pathways for the formation of  
772 secondary sulfate aerosols, N<sub>2</sub>O and potential HONO.

773 Results from this study have important atmospheric implications. Firstly, the results  
774 suggest that the heterogeneous conversion of SO<sub>2</sub> in the atmosphere will be affected by  
775 the availability of nitrate, and further emphasize that the complexity of the reaction of  
776 SO<sub>2</sub> on mineral dust. This chemistry may occur on surfaces of airborne dust particles that  
777 are known to be transported and play a role in the chemistry of the troposphere, which  
778 would affect the estimation of the amount of global atmospheric sulfate, and further

779 affect the previously estimated radiative forcing and cooling effect of sulfate aerosols in  
780 the atmosphere (Dentener et al., 1996). Secondly, Fe (II) in airborne particles has been  
781 observed (Zhu et al., 1997; Zhuang et al., 2001) and its concentration in dust increased  
782 continuously during long-range transport (Zhuang et al., 2001). Also, in the real  
783 atmospheric systems, sulfuric acid is a common component of particles (Finlayson-Pitts  
784 and Pitts, 2000).  $PM_{2.5}$  is generally acidic due to partial neutralization of acidic sulfate  
785 and nitrate under some atmospheric conditions (Huang et al., 2011), and even dust  
786 particle might become acidified to  $pH < 2$  in the troposphere (Meskhidze et al., 2003).  
787 The Fe (II)-containing airborne particles will inevitably be loaded by nitrate and be  
788 acidified through contact with acidic particles such as sulfuric acid aerosols and acidic  
789  $PM_{2.5}$  particles, or become the heterogeneous reaction interface of  $SO_2$  and  $NO_2$  in the  
790 atmosphere. Hence, we can expect the production of potential HONO during these  
791 processes. The results presented here may imply that such a heterogeneous conversion  
792 pathway of low concentration  $SO_2$  on nitrate-containing airborne dust particles may be a  
793 potential and yet unknown daytime and nighttime significant source of HONO, and  
794 reveal that the presence of nitrate on mineral dust aerosol may play a role in the  
795 chemistry of HONO in the troposphere. In the meantime, these particles containing  
796 potential HONO may become the oxidizing carriers for the oxidation of atmospheric  
797 reduced gases, and thereby enhance the atmospheric oxidation ability. Understanding this  
798 chemistry will contribute to the elucidation of the potential contribution of the unreleased  
799 HONO in the particle for the conversion of  $SO_2$  and the enhanced formation of sulfate in  
800 the atmosphere in the daytime and at night. Finally, several studies indicated that the  
801 photolysis of aqueous nitrate (Dubowski et al., 2001; Roca et al., 2008) and adsorbed

802 nitrate (Schuttlefield et al., 2008) is a source of NO<sub>x</sub> (i.e., NO + NO<sub>2</sub>), OH radicals and O  
803 (<sup>3</sup>P). All of these products represent highly reactive oxidants in the gas phase and in other  
804 environmentally relevant phases. The production of hydroxyl radicals will favor the  
805 conversion of SO<sub>2</sub> to particulate sulfate, while the photolysis of aqueous or adsorbed  
806 nitrate will lead to a loss of nitrate in the particulate phase. Furthermore, according to our  
807 experimental results and discussion above, low to moderate amounts of nitrate will  
808 significantly promote the heterogeneous conversion of SO<sub>2</sub> and the formation of sulfate  
809 on airborne hematite-containing mineral dust particles, while the heterogeneous uptake of  
810 SO<sub>2</sub> on nitrate-containing mineral dust in the atmosphere will also bring a loss of  
811 adsorbed nitrate on the particle surface with the concomitant formation of gas-phase  
812 products including HONO and N<sub>2</sub>O. Therefore, these studies mentioned above will aid in  
813 understanding the negative linear correlation between sulfate and nitrate contents in  
814 ambient particles (Kong et al., 2014). However, the reasons for the negative correlation  
815 are unknown. There is still lack of corresponding research on the formation mechanism  
816 of the negative correlation up to now, and all these aspects need to be further investigated.

817

818 **Supplementary material related to this article is available online at**

819 **[http://www.atmos-chem-phys-discuss.net/14/11577/2014/acpd-14-11577-2014-](http://www.atmos-chem-phys-discuss.net/14/11577/2014/acpd-14-11577-2014-supplement.pdf)**  
820 **supplement.pdf.**

821

822 *Acknowledgements.* This work was supported by the National Natural Science  
823 Foundation of China (Grant Nos. 21277028, 40775079, 21190053 and 41275126) and the

824 Scientific Research Foundation for the Returned Overseas Chinese Scholars, State  
825 Education Ministry.

826 **References**

827 Ansari, A., Peral, J., Domènech, X., and Rodríguez-Clemente, R.: Oxidation of  $\text{HSO}_3^-$  in  
828 aqueous suspensions of  $\alpha\text{-Fe}_2\text{O}_3$ ,  $\alpha\text{-FeOOH}$ ,  $\beta\text{-FeOOH}$  and  $\gamma\text{-FeOOH}$  in the dark and  
829 under illumination, *Environ. Pollut.*, 95, 283–288, 1997.

830 Arens, F., Gutzwiller, L., Baltensperger, U., Gägler, H. W., and Ammann, M.:  
831 Heterogeneous reaction of  $\text{NO}_2$  on diesel soot particles, *Environ. Sci. Technol.*, 35,  
832 2191–2199, 2001.

833 Baltrusaitis, J., Cwiertny, D. M., and Grassian, V. H.: Adsorption of sulfur dioxide on  
834 hematite and goethite particle surfaces, *Phys. Chem. Chem. Phys.*, 9, 5542–5554, 2007.

835 Behra, P. and Sigg, L.: Evidence for redox cycling of iron in atmospheric water droplets,  
836 *Nature*, 344, 419–421, 1990.

837 Börensén, C., Kirchner, U., Scheer, V., Vogt, R., and Zellner R.: Mechanism and kinetics  
838 of the reactions of  $\text{NO}_2$  or  $\text{HNO}_3$  with alumina as a mineral dust model compound, *J.*  
839 *Phys. Chem. A*, 104, 5036–5045, 2000.

840 Burley, J. D., and Johnston, H. S.: Ionic mechanisms for heterogeneous stratospheric  
841 reactions and ultraviolet photoabsorption cross sections for  $\text{NO}_2^+$ ,  $\text{HNO}_3$ , and  $\text{NO}_3^-$  in  
842 sulfuric acid, *Geophys. Res. Lett.*, 19, 1359–1361. 1992.

843 Chun, K. C. and Quon, J. E.: Capacity of ferric oxide particles to oxidize sulfur dioxide in  
844 air, *Environ. Sci. Technol.*, 7, 532–538, 1973.

845 Dentener, F. J., Carmichael, G. R., Zhang, Y., Lelieveld, J., and Crutzen, P. J.: Role of  
846 mineral aerosol as a reactive surface in the global troposphere, *J. Geophys Res.*, 101,  
847 22869–22889, 1996.

848 Drescher, S. R. and Brown, S. D.: Solid phase microextraction-gas chromatographic–  
849 mass spectrometric determination of nitrous oxide evolution to measure denitrification  
850 in estuarine soils and sediments, *J. Chromatogr. A*, 1133, 300–304, 2006.

851 Dubowski, Y., Colussi, A. J., and Hoffmann, M. R.: Nitrogen dioxide release in the 302  
852 nm band photolysis of spray-frozen aqueous nitrate solutions, *Atmospheric*  
853 *implications*, *J. Phys. Chem. A*, 105, 4928–4932, 2001.

854 Egashira, M., Nakashima, M., Kawasumi, S., and Seyama, T.: Temperature  
855 programmed desorption study of water adsorbed on metal oxides. 2. Tin oxide surfaces,  
856 *J. Phys. Chem.*, 85, 4125–4130, 1981.

857 Faguy, P. W. and Marinković, N. S.: An in situ infrared study on the effect of pH on  
858 anion adsorption at Pt (111) electrodes from acid sulfate solutions, *Langmuir*, 12, 243–  
859 247, 1996.

860 Finlayson-Pitts, B. J., and Pitts, J. N.: *Chemistry of the upper and lower atmosphere:*  
861 *Theory, experiments, and applications*, Academic Press, San Diego, CA, 2000.

862 Finlayson-Pitts, B. J., Wingen, L. M., Sumner, A. L., Syomin, D., and Ramazan, K. A.:  
863 The heterogeneous hydrolysis of NO<sub>2</sub> in laboratory systems and in outdoor and indoor  
864 atmospheres: An integrated mechanism, *Phys. Chem. Chem. Phys.*, 5, 223–242, 2003.

865 Fu, H., Wang, X., Wu, H., Yin, Y., and Chen, J.: Heterogeneous uptake and oxidation of  
866 SO<sub>2</sub> on iron oxides, *J. Phys. Chem. C*, 111, 6077–6085, 2007.

867 Goodman, A. L., Li, P., Usher, C. R., and Grassian, V. H.: Heterogeneous uptake of  
868 sulfur dioxide on aluminum and magnesium oxide particles, *J. Phys. Chem. A*, 105,  
869 6109–6120, 2001.

870 Goodman, A. L., Underwood, G. M., and Grassian, V. H.: A spectroscopic investigation  
871 of the heterogeneous reaction  $2\text{NO}_2 + \text{H}_2\text{O} (\text{a}) \rightarrow \text{HONO}(\text{g}) + \text{HNO}_3 (\text{a})$  on hydrated  
872 silica Particles: Characterization of gas-phase and adsorbed products, *J. Phys. Chem. A*,  
873 103, 7217–7223, 1999.

874 Harris, E., Sinha, B., van Pinxteren, D., Tilgner, A., Fomba, K. W., Schneider, J., Roth,  
875 A., Gnauk, T., Fahlbusch, B., Mertes, S., Lee, T., Collett, J., Foley, S., Borrmann, S.,  
876 Hoppe, P., and Herrmann, H.: Enhanced role of transition metal ion catalysis during in-  
877 cloud oxidation of SO<sub>2</sub>, *Science*, 340, 727–730, 2013.

878 Hixson, B. C., Jordan, J. W., Wagner, E. L., and Holly M.: Reaction products and  
879 kinetics of the reaction of NO<sub>2</sub> with  $\gamma\text{-Fe}_2\text{O}_3$ , *J. Phys. Chem. A*, 115, 13364–13369,  
880 2011.



881 Ho, K. F., Lee, S. C., Chan, C. K., Yu, J. C., Chow, J. C., and Yao, X. H.:  
882 Characterization of chemical species in PM<sub>2.5</sub> and PM<sub>10</sub> aerosols in Hong Kong, *Atmos.*  
883 *Environ.*, 37, 31–39, 2003.

884 Hoffman, R. C., Laskin, A., and Finlayson-Pitts, B. J.: Sodium nitrate particles: physical  
885 and chemical properties during hydration and dehydration, and implications for aged  
886 sea salt aerosols, *J. Aerosol Sci.*, 35, 869–887, 2004.

887 Huang, X., Qiu, R., Chan, C. K., and Kant, P. R.: Evidence of high PM<sub>2.5</sub> strong acidity  
888 in ammonia-rich atmosphere of Guangzhou, China: Transition in pathways of ambient  
889 ammonia to form aerosol ammonium at  $[\text{NH}_4^+]/[\text{SO}_4^{2-}]=1.5$ , *Atmos. Res.*, 99, 488–495,  
890 2011.

891 Hug, S. J.: In situ Fourier transform infrared measurements of sulfate adsorption on  
892 hematite in aqueous solutions, *J. Colloid Interface Sci.*, 188, 415–422, 1997.

893 Hussain, G. and Rahman, M. M.: An infrared study of co-adsorption of N<sub>2</sub>O and CO on  
894 ZnO, *Spectrochim. Acta*, 64A, 880–885, 2006.

895 Jickells, T. D. and Spokes, L. J.: Atmospheric iron inputs to the ocean, in: the  
896 biogeochemistry of iron in seawater, edited by: Turner, D. R. and Hunter, K. A.,  
897 SCOR-IUPAC Series, J. Wiley, Baltimore, 85–121, 2001.

898 Kasibhatla, P., Chameides, W. L., and St John, J.: A three-dimensional global model  
899 investigation of seasonal variations in the atmospheric burden of anthropogenic sulfate  
900 aerosols, *J. Geophys. Res.*, 102, 3737–3759, 1997.

901 Kerminen, V., Pirjola, L., Boy, M., Eskola, A., Teinilä K., Laakso, L., Asmi, A., Hienola,  
902 J., Lauri, A., Vainio, V., Lehtinen, K., and Kulmala, M.: Interaction between SO<sub>2</sub> and  
903 submicron atmospheric particles, *Atmos. Res.*, 54, 41–57, 2000.

904 Kleffmann, J., Gavriloaiei, T., Hofzumahaus, A., Holland, F., Koppmann, R., Rupp, L.,  
905 Schlosser, E., Siese, M., and Wahner, A.: Daytime formation of nitrous acid: A major  
906 source of OH radicals in a forest, *Geophys. Res. Lett.*, 32, L05818, doi:  
907 10.1029/2005GL022524, 2005.

908 Kong, L., Yang, Y., Zhang, S., Zhao, X., Du, H., Fu, H., Zhang, S., Cheng, T., Yang, X.,  
909 Chen, J., Wu, D., Shen, J., Hong, S., and Jiao, L.: Observations of linear dependence  
910 between sulfate and nitrate in atmospheric particles, *J. Geophys. Res.*, 119, 341–361,  
911 2014.

912 Laskin, A., Gaspar, D. J., Wang, W. H., Hunt, S. W., Cowin, J. P., Colson, S. D., and  
913 Finlayson-Pitts, B. J.: Reactions at interfaces as a source of sulfate formation in sea-  
914 salt particles, *Science*, 301, 340–344, 2003.

915 Lin, L., Kong, L., Chen, J., Experimental study of the effects of ammonium nitrate on  
916 SO<sub>2</sub> gas-particle transfer on the surface of atmospheric aerosols, *Chem. J. Chinese U.*,  
917 31, 751-755, 2010.

918 Liu, C., Ma, Q., Liu, Y., Ma, J., and He, H.: Synergistic reaction between SO<sub>2</sub> and NO<sub>2</sub>  
919 on mineral oxides: A potential formation pathway of sulfate aerosol, *Phys. Chem.*  
920 *Chem. Phys.*, 14, 1668–1676, 2012.

- 921 Luria, M. and Sievering, H.: Heterogeneous and homogeneous oxidation of SO<sub>2</sub> in the  
922 remote marine atmosphere, *Atmos. Environ.*, 25, 1489–1496, 1991.
- 923 Martin, L. R., Damschen, D. E., and Judeikis, H. S.: The reactions of nitrogen oxides  
924 with SO<sub>2</sub> in aqueous aerosols, *Atmos. Environ.*, 15, 191–195, 1981.
- 925 McCurdy, P. R., Hess, W. P., and Sotiris S.: Nitric Acid-Water Complexes: Theoretical  
926 Calculations and Comparison to Experiment, *J. Phys. Chem. A*, 106, 7628–7635, 2002.
- 927 Meskhidze, N., Chameides, W. L., Nenes, A., and Chen, G.: Iron mobilization in mineral  
928 dust: Can anthropogenic SO<sub>2</sub> emissions affect ocean productivity?, *Geophys. Res. Lett.*,  
929 30, 2085-2089, 2003.
- 930 Moore, J. K., Doney, S. C., Glover, D. M., and Fung, I. Y.: Iron cycling and nutrient-  
931 limitation patterns in surface waters of the World Ocean, *Deep Sea Res., Part II*, 49 (1-  
932 3), 463–507, 2002.
- 933 Nanayakkara, C. E., Pettibone, J., and Grassian, V. H.: Sulfur dioxide adsorption and  
934 photooxidation on isotopically-labeled titanium dioxide nanoparticle surfaces: Roles of  
935 surface hydroxyl groups and adsorbed water in the formation and stability of adsorbed  
936 sulfite and sulfate, *Phys. Chem. Chem. Phys.*, 14, 6957–6966, 2012.
- 937 Peak, D., Ford, R. G., and Sparks, D.: An in situ ATR-FTIR investigation of sulfate  
938 bonding mechanisms on goethite, *J. Colloid Interface Sci.*, 218, 289–299, 1999.

939 Persson, P. and Lovgren, L.: Potentiometric and spectroscopic studies of sulfate  
940 complexation at the goethite-water interface, *Geochim. Cosmochim. Ac.*, 60, 2789–  
941 2799, 1996.

942 Pires, M., Van Den Bergh, H., and Rossi, M. J.: The heterogeneous formation of N<sub>2</sub>O  
943 over bulk condensed phases in the presence of SO<sub>2</sub> at high humidities, *J. Atmos.*  
944 *Chem.*, 25, 229–250, 1996.

945 Pires, M., Van Den Bergh, H., and Rossi, M. J.: The heterogeneous formation of N<sub>2</sub>O in  
946 the presence of acidic solutions: Experiments and modeling, *Int. J. Chem. Kinet.*, 29,  
947 869–891, 1997.

948 Pitts, J. N. Jr., Sanhueza, E., Atkinson, R., Carter, W. P. L., Winer, A. M., Harris, G. W.,  
949 and Plum, C. N.: An investigation of the dark formation of nitrous acid in  
950 environmental chambers, *Int. J. Chem. Kinet.*, 16, 919–939, 1984.

951 Preszler Prince, A., Kleiber, P. D., Grassian, V. H., and Young, M. A.: Heterogeneous  
952 interactions of calcite aerosol with sulfur dioxide and sulfur dioxide/nitric acid  
953 mixtures, *Phys. Chem. Chem. Phys.*, 9, 3432–3439, 2007.

954 Ramazan, K. A., Wingen, L. M., Miller, Y., Chaban, G. M., Gerber, R. B., Xantheas, S.  
955 S., and Finlayson-Pitts, B. J.: New experimental and theoretical approach to the  
956 heterogeneous hydrolysis of NO<sub>2</sub>: Key role of molecular nitric acid and its complexes,  
957 *J. Phys. Chem. A*, 110, 6886–6897, 2006.

958 Rivera-Figueroa, A. M., Sumner, A. L., and Finlayson-Pitts, B. J.: Laboratory studies of  
959 potential mechanisms of renoxification of tropospheric nitric acid, *Environ. Sci.*  
960 *Technol.*, 37, 548–554, 2003.

961 Roca, M., Zahardis, J., Bone, J., El-Maazawi, M., and Grassian, V. H.: 310 nm irradiation  
962 of atmospherically relevant concentrated aqueous nitrate solutions: Nitrite production  
963 and quantum yields, *J. Phys. Chem. A*, 112, 13275–13281, 2008.

964 Schuttlefield, J., Rubasinghege, G., El-Maazawi, M., Bone, J., and Grassian, V. H.:  
965 Photochemistry of adsorbed nitrate, *J. Am. Chem. Soc.*, 130, 12210–12211, 2008.

966 Schwertmann, U., and Cornell, R. M.: *Iron oxides in the laboratory: Preparation and*  
967 *characterization*, Wiley-VCH, New York, 2000.

968 Seinfeld, J. H. and Pandis, S. N.: *Atmospheric Chemistry and Physics: From Air*  
969 *Pollution to Climate Change*, 2nd edn., John Wiley & Sons Inc., New York, 2006.

970 Shi, Z., Bonneville, S., Krom, M. D., Carslaw, K. S., Jickells, T. D., Baker, A. R., and  
971 Benning, L. G.: Iron dissolution kinetics of mineral dust at low pH during simulated  
972 atmospheric processing, *Atmos. Chem. Phys.*, 11, 995–1007, doi:10.5194/acp-11-995-  
973 2011, 2011.

974 Sugimoto, T. and Wang, Y.: Mechanism of the shape and structure control of  
975 monodispersed  $\alpha$ -Fe<sub>2</sub>O<sub>3</sub> particles by sulfate ions, *J. colloid interface sci.*, 207, 137–149,  
976 1998.

977 Summers, D. P.: Ammonia formation by the reduction of nitrite/nitrate by FeS: Ammonia  
978 formation under acidic conditions, *Origins Life Evol. B.*, 35, 299–312, 2005.

979 Ullerstam, M., Johnson, M. S., Vogt, R., and Ljungstrom, E.: DRIFTS and Knudsen cell  
980 study of the heterogeneous reactivity of SO<sub>2</sub> and NO<sub>2</sub> on mineral dust, *Atmos. Chem.*  
981 *Phys.*, 3, 2043–2051, doi:10.5194/acp-3-2043-2003, 2003.

982 Ullerstam, M., Vogt, R., Langer, S., and Ljungström, E.: The kinetics and mechanism of  
983 SO<sub>2</sub> oxidation by O<sub>3</sub> on mineral dust, *Phys. Chem. Chem. Phys.*, 4, 4694–4699, 2002.

984 Underwood, G. M., Miller, T. M., and Grassian, V. H.: Transmission FT-IR and Knudsen  
985 cell study of the heterogeneous reactivity of gaseous nitrogen dioxide on mineral oxide  
986 particles, *J. Phys. Chem. A*, 103, 6184–6190, 1999.

987 Usher, C. R., Al-Hosney, H., Carlos-Cuellar, S., and Grassian, V. H.: A laboratory study  
988 of the heterogeneous uptake and oxidation of sulfur dioxide on mineral dust particles, *J.*  
989 *Geophys. Res.*, 107, 4713–4721, 2002.

990 Usher, C. R., Michel, A. E., and Grassian, V. H.: Reactions on mineral dust, *Chem. Rev.*,  
991 103, 4883–4939, 2003.

992 Watanabe, H., Gutleben, C. D., and Seto, J.: Sulfate ions on the surface of maghemite and  
993 hematite, *Solid State Ionics*, 69, 29–35, 1994.

994 Wiesen, P., Kleffmann, J., Kurtenbach, R., and Becker, K. H.: Mechanistic study of the  
995 heterogeneous conversion of NO<sub>2</sub> into HONO and N<sub>2</sub>O on acid surfaces, *Faraday*  
996 *Discuss.*, 100, 121–127, 1995.

- 997 Wingen, L. M., Barney, W. S., Lakin, M. J., Brauers, T., and Finlayson-Pitts, B. J.: A  
998 unique method for laboratory quantification of gaseous nitrous acid (HONO) using the  
999 reaction  $\text{HONO} + \text{HCl} \rightarrow \text{ClNO} + \text{H}_2\text{O}$ , *J. Phys. Chem. A*, 104, 329–335, 2000.
- 1000 Wu, L. Y., Tong, S. R., Wang, W. G., and Ge, M. F.: Effects of temperature on the  
1001 heterogeneous oxidation of sulfur dioxide by ozone on calcium carbonate, *Atmos.*  
1002 *Chem. Phys.*, 11, 6593–6605, doi:10.5194/acp-11-6593-2011, 2011.
- 1003 Yamaguchi, T., Jin, T., and Tanabe, K.: Structure of acid sites on sulfur-promoted iron  
1004 oxide, *J. Phys. Chem.*, 90, 3148–3152, 1986.
- 1005 Zhang, Q. J., Wang, X., Chen, J. M., and Zhuang, G. S.: Formation of Fe (II) (aq) and  
1006 sulfate via heterogeneous reaction of  $\text{SO}_2$  with  $\text{Fe}_2\text{O}_3$ , *Chem. J. Chinese U.*, 7, 1347–  
1007 1350, 2007.
- 1008 Zhang, X., Zhang, G., Chen, J., Wang, Y., Wang, X., An, Z., and Zhang, P.:  
1009 Heterogeneous reactions of sulfur dioxide on typical mineral particles, *J. Phys. Chem.*  
1010 *B*, 110, 12588–12596, 2006.
- 1011 Zhu T., Shang J., and Zhao D. F.: The roles of heterogeneous chemical processes in the  
1012 formation of an air pollution complex and gray haze, *Sci. China Chem.*, 54, 145–153,  
1013 2011.
- 1014 Zhu, X. R., Prospero, J. M., and Millero, F. J.: Diel variability of soluble Fe (II) and  
1015 soluble total Fe in North African dust in the trade winds at Barbados, *J. Geophys. Res.*,  
1016 102, 21297–21306, 1997.

1017 Zhuang, G., Yi, Z., Duce, R. A., and Brown, P. R.: Link between iron and sulphur cycles  
1018 suggested by detection of Fe (II) in remote marine aerosols, *Nature*, 355, 537–539,  
1019 1992.

1020 Zhuang, G. S., Guo, J. H., Yuan, H., and Zhao, C. Y.: The compositions, sources, and  
1021 size distribution of the dust storm from China in spring 2000 and its impact on the  
1022 global environment, *Chinese Sci. Bull.*, 46, 895–901, 2001.

1023

1024

1025

1026

1027

1028

1029

1030

1031

1032

1033

1034



1035

1036

1037

1038 **Table 1.** Assignment of vibrational frequencies of surface species formed on hematite

1039 particle surfaces and on hematite-nitrate mixtures surfaces.

Surface species	Hematite (cm <sup>-1</sup> )	Hematite-nitrate mixture (cm <sup>-1</sup> )
SO <sub>3</sub> <sup>2-</sup> /HSO <sub>3</sub> <sup>-</sup>	1056	1080, 1050, 966
SO <sub>4</sub> <sup>2-</sup>	1361, 1337, 1261, 1158, 1056, 1000	1158, 1190, 987
Acidic species	1219	
NO <sub>3</sub> <sup>-</sup>		1599, 1587, 1567
NO <sub>2</sub> <sup>-</sup>		1506, 1487
Adsorbed HNO <sub>3</sub>		1676, 1686, 1697, 1716
O-H region	3664, 3631	3664, 3631

1040

1041

1042

1043

1044

1045

1046

1047

1048 **Table 2.** Sulfate formation rates and uptake coefficients for heterogeneous reactions of  
 1049 SO<sub>2</sub> on hematite and the hematite-nitrate mixtures at 298 K.

	NaNO <sub>3</sub> (%)	A <sub>BET</sub> (m <sup>2</sup> /g)	Sulfate formation rate (ions s <sup>-1</sup> ) (×10 <sup>15</sup> )	A <sub>geometric</sub> (m <sup>2</sup> ) (×10 <sup>5</sup> )	γ <sub>BET</sub> (×10 <sup>7</sup> )	γ <sub>geometric</sub> (×10 <sup>3</sup> )
1050	0	12.1	1.28±0.07	7.85	5.58±0.29	2.58±0.14
1051	2	11.8	1.48±0.15	7.85	6.60±0.69	2.98±0.31
1052	4	11.7	2.01±0.12	7.85	9.04±0.56	4.04±0.25
1053	6	11.5	3.62±0.18	7.85	16.6±0.81	7.29±0.35
1054	12	10.9	4.93±0.29	7.85	23.8±0.14	9.93±0.58
1055	24	9.1	7.11±1.34	7.85	41.2±0.78	14.3±2.69
	48	5.2	4.39±0.39	7.85	44.5±0.39	8.84±0.78
	60	4.0	1.62±0.25	7.85	21.3±0.32	3.25±0.49
1056	72	2.8	0.59±0.15	7.85	11.2±0.29	1.19±0.31
	90	1.3	0.15±0.03	7.85	6.10±1.05	0.30±0.05
1057	100		0		0	0

1058

1059

1060

1061

1062

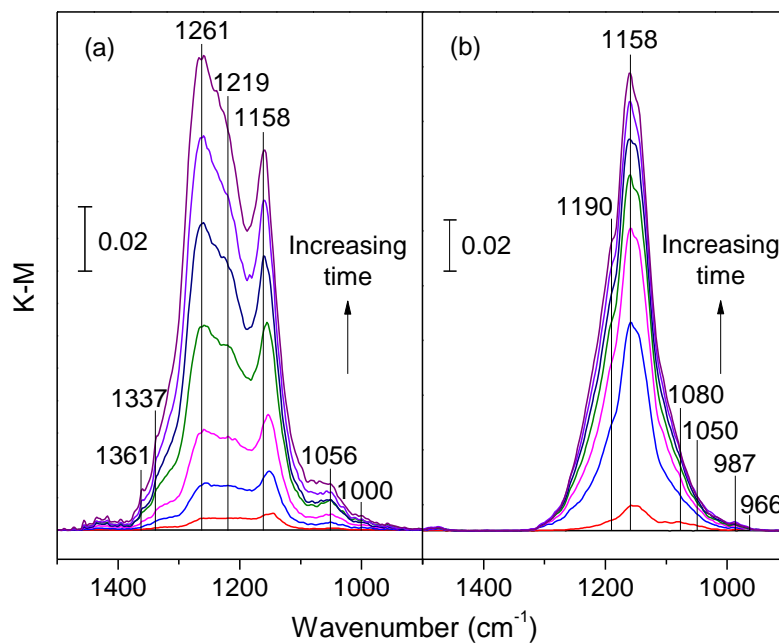
1063

1064

1065

1066

1067



1068

1069 **Fig. 1.** DRIFT spectra of different samples recorded upon exposure to SO<sub>2</sub> at 298 K. **(a)**

1070 hematite. **(b)** FN-24.

1071

1072

1073

1074

1075

1076

1077

1078

1079

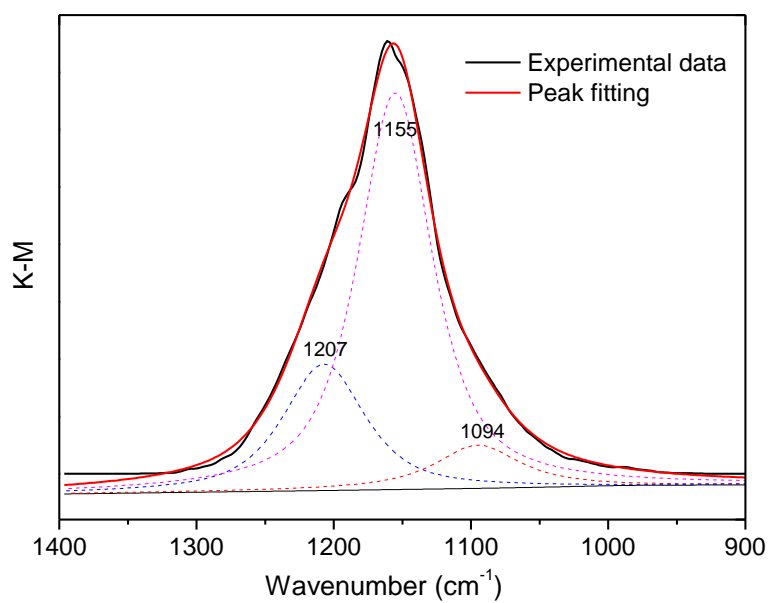
1080

1081

1082

1083

1084



1085 **Fig. 2.** Peak fitting of the last DRIFT spectrum of the products on FN-24 shown in Fig. 1  
1086 by mixed Gaussian-Lorentzian peak fitting.

1087

1088

1089

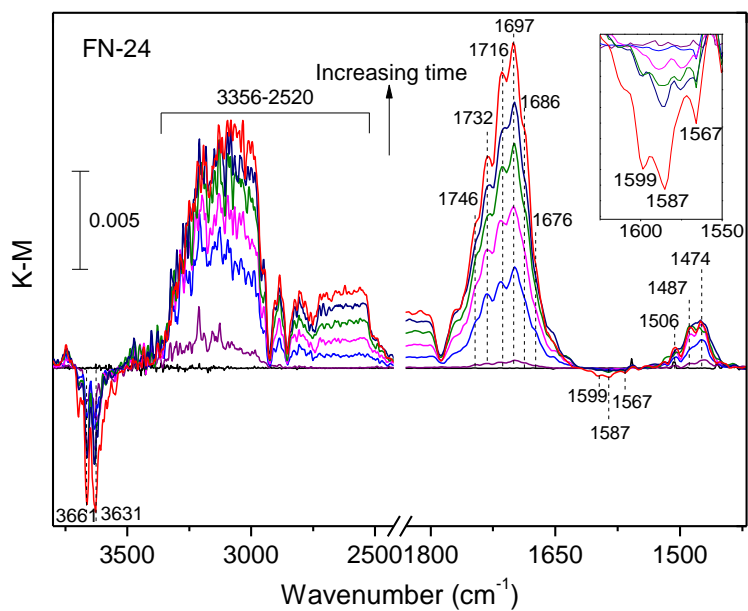
1090

1091

1092

1093

1094



1095

1096 **Fig. 3.** DRIFT spectra of FN-24 as a function of time after exposure to SO<sub>2</sub> in the range

1097 of 3800 to 1350 cm<sup>-1</sup>. The inset shows expanded region from 1630 to 1550 cm<sup>-1</sup>.

1098

1099

1100

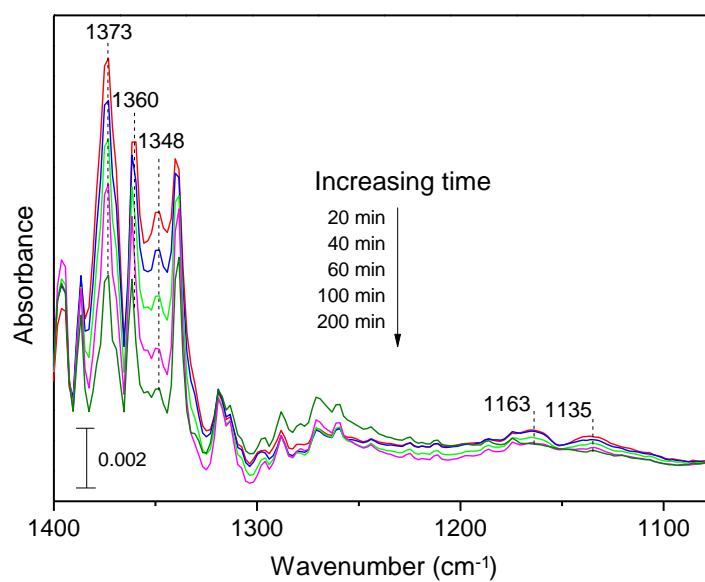
1101

1102

1103

1104

1105



1106

1107 **Fig. 4.** In situ White cell-FTIR spectra of FN-24 recorded upon exposure to 50 ppm SO<sub>2</sub>

1108 + 21% O<sub>2</sub> at room temperature for different reaction times.

1109

1110

1111

1112

1113

1114

1115

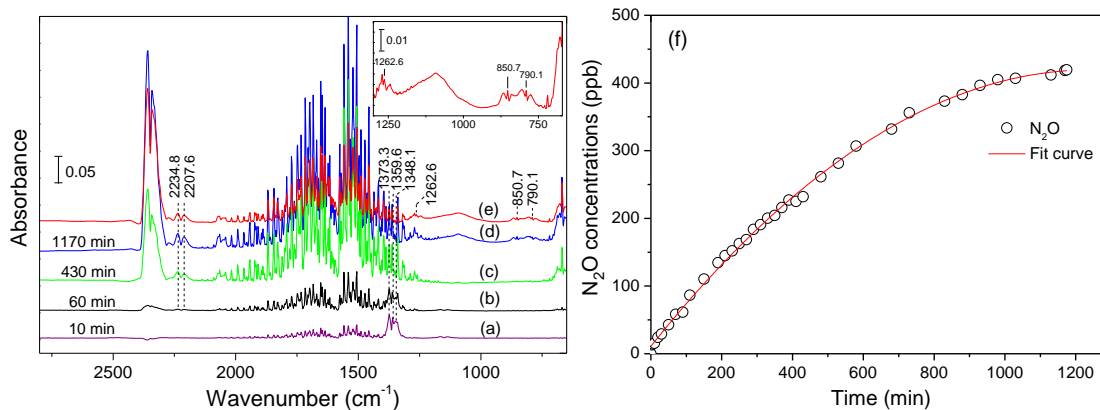
1116

1117

1118

1119

1120



1121

1122 **Fig. 5.** In situ FTIR spectra of FN-90 recorded upon exposure to 12.5 ppm SO<sub>2</sub> + 21% O<sub>2</sub>

1123 at room temperature for different times. (a) 10 min. (b) 60 min. (c) 430 min. (d) 1170

1124 min. (e) difference spectrum: (d) minus (c). (f) The concentration of the formed N<sub>2</sub>O as a

1125 function of time during the reaction of FN-90 sample with SO<sub>2</sub>.

1126

1127

1128

1129

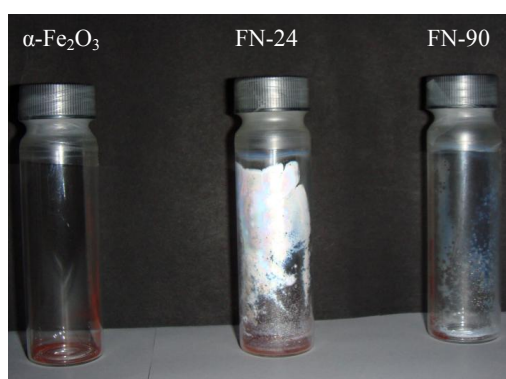
1130

1131

1132

1133

1134



1135

1136

1137 **Fig. 6.** Digital photos of different samples after reaction with 50 ppm  $\text{SO}_2$  +21%  $\text{O}_2$  in the  
1138 dark at 298 K for about 7 days.

1139

1140

1141

1142

1143



1144

1145

1146

1147

1148

1149

1150

1151

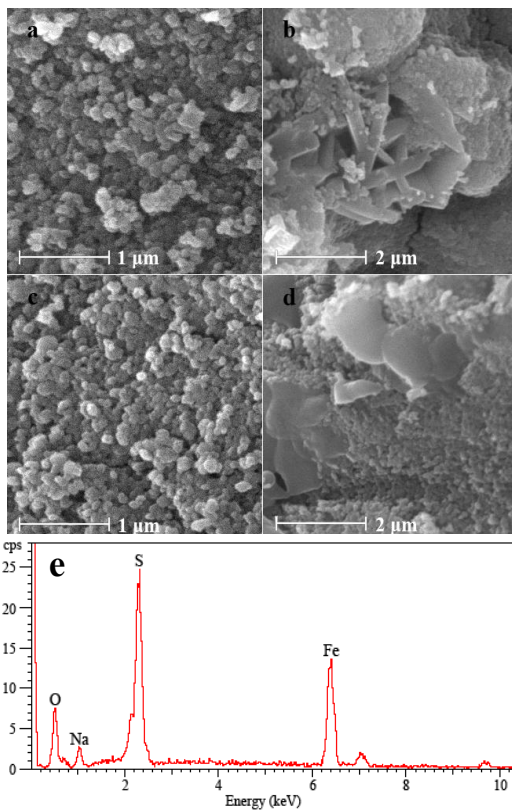
1152

1153

1154

1155

1156



1157 **Fig. 7.** SEM images and EDX spectrum. Top panels: SEM images of FN-24 (**a, b**) and  
1158 FN-90 (**c, d**) particles before (left) and after (right) exposure to 3 ppm SO<sub>2</sub> at 298 K for  
1159 240 min. Bottom panel: typical EDX spectrum of the flaky substance.

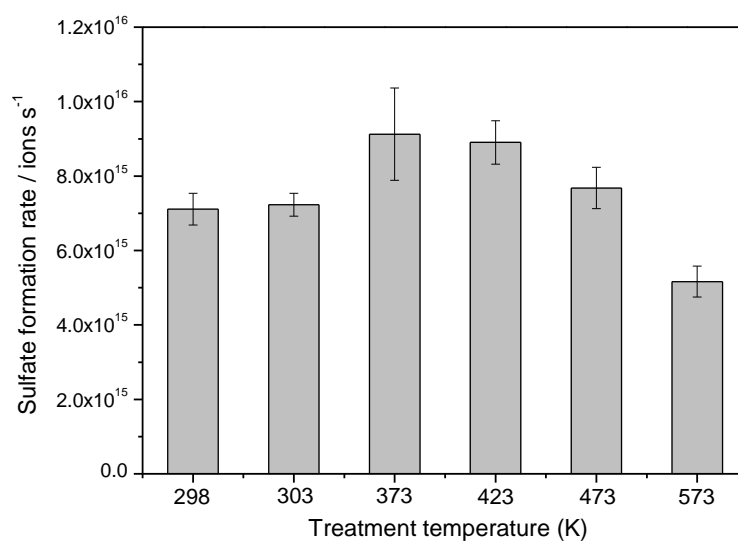
1160

1161

1162

1163

1164



1165

1166 **Fig. 8.** Sulfate formation rates on 30 mg of FN-24 after exposure to 3 ppm SO<sub>2</sub> under

1167 different pre-treatment temperatures.

1168

1169

1170

1171

1172

1173

1174

1175

1176

1177

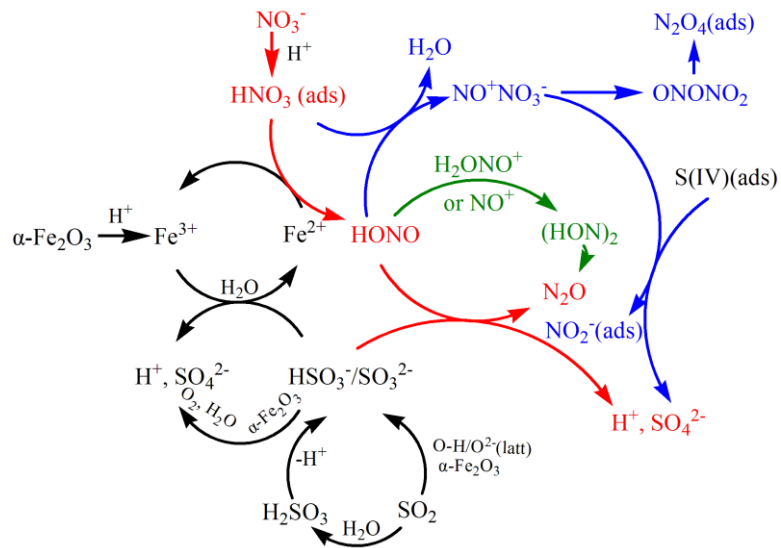
1178

1179

1180

1181

1182



1183 **Fig. 9.** Schematic of the reaction mechanism of the heterogeneous oxidation of SO<sub>2</sub> on  
1184 hematite in the presence of nitrate.

1185

1186

1187

1188